The perigranitic W-Au Salau deposit (Pyrenees, France): polyphase genesis of a late Variscan intrusion related deposit

Thomas Poitrenaud, Eric Marcoux, Romain Augier, Marc Poujol

BSGF - Earth Sciences Bulletin 2021, 192, 22

https://doi.org/10.1051/bsgf/2020044

Special Issue Minéralisations périgranitiques ed. E. Marcoux

Available online at:
www.bsgf.fr

OPEN ACCESS

The perigranitic W-Au Salau deposit (Pyrenees, France): polyphase genesis of a late Variscan intrusion related deposit

Thomas Poitrenaud[1,2,3,*], Éric Marcoux[1,2,3], Romain Augier[1,2,3] and Marc Poujol[4]

[1] Université d'Orléans, ISTO, UMR 7327, 45071 Orléans, France
[2] CNRS/INSU, ISTO, UMR 7327, 45071 Orléans, France
[3] BRGM, ISTO, UMR 7327, BP 36009, 45060 Orléans, France
[4] Univ. Rennes, CNRS, Géosciences Rennes – UMR 6118, F-35000 Rennes, France

Received: 26 May 2020 / Accepted: 10 December 2020 / Publishing online: 16 April 2021

Abstract – A field study combined with a laboratory study and 3D modeling have been performed in order to decipher the genesis of the Salau deposit W-Au mineralization (Pyrenees, France), one of the most important for tungsten in Europe. Results show the existence of two superimposed ore types, emplaced ca. 10 km depth and within decreasing temperature conditions: a calcic silicates skarn with rare scheelite and disseminated sulphides followed by a mineralized breccia with massive sulphides (pyrrhotite and chalcopyrite dominant), coarse-grained scheelite and gold, representing the main part of the ore mined in the past. This breccia is localized in ductile-brittle shear-zones which crosscut the granodiorite. U/Pb dating on zircon, apatite and scheelite, previously realized, confirmed this polyphase evolution. These two types of mineralization, linked to the emplacement of two successive intrusions as confirmed by sulphur isotopic analysis, granodioritic then leucogranitic, can be classified as belonging to the Intrusion-Related Gold Deposit type (IRGD). The emplacement of the high-grade gold and scheelite breccia was initiated by the progressive localization of the regional deformation in the Axial Zone of the Pyrenees during the Permian within E-W dextral-reverse faults.

Keywords: Skarn / Pyrenees / scheelite / tungsten / gold / Salau / IRGD

Résumé – Le gisement périgranitique à W-Au de Salau (Pyrénées, France) : histoire polyphasée d'un système minéralisé tardi-varisque. Une étude de terrain combinée à une étude de laboratoire et de modélisation 3D a été réalisée afin de décrypter la genèse de la minéralisation à W-Au du gisement de Salau (Pyrénées, France), une des plus importantes d'Europe pour le tungstène. Les résultats montrent qu'il existe deux types de minéralisations superposées, mises en place vers 10 km de profondeur et dans des conditions décroissantes de température : un skarn à silicates calciques, rare scheelite et sulfures disséminés, suivi d'une brèche filonienne à sulfures massifs (pyrrhotite et chalcopyrite dominante), scheelite grossière et or qui a constitué l'essentiel du minerai lors de la phase d'exploitation. Cette brèche se localise dans une série de zones de cisaillement ductile-fragile recoupant l'intrusion granodioritique. Les datations U/Pb sur zircon, apatite et scheelite réalisées antérieurement, confirment ce polyphasage. Ces deux minéralisations, associées à deux intrusions successives comme le confirment les analyses isotopiques du soufre, granodioritique puis leucogranitique, s'inscrivent dans l'évolution d'un modèle Intrusion Related Gold Deposit. La mise en place de la brèche filonienne à forte teneur en or et scheelite est initiée par la localisation progressive de la déformation régionale dans la Zone axiale des Pyrénées durant le Permien au sein de failles E-W dextres inverses.

Mots clés : Skarn / Pyrénées / scheelite / tungstène / or / Salau / IRGD

*Corresponding author: thomas.poitrenaud@hotmail.fr

1 Introduction

During the last twenty years, new metallogenic models have been proposed, such as the Intrusion Related Gold Deposit model (Lang and Baker, 2001; Hart, 2007) or the Carlin type gold deposit model (Kesler *et al.*, 2005), in particular thanks to the use of innovative techniques which enable to re-examine known deposits: isotopic geochemistry (Raju *et al.*, 2015; Mao *et al.*, 2016), geochronology (Charles *et al.*, 2013; Ballouard *et al.*, 2017; Harlaux *et al.*, 2018), thermicity (Delchini *et al.*, 2016; Poitrenaud, 2018) or 3D modeling (Cowan, 2020). The complexity of the deposits often reveals a polyphase of the mineralization, previously often described as resulting from a single mineralizing event (Lefebvre *et al.*, 2018). Although comprising numerous historically exploited deposits and a significant mining potential, the Pyrenean segment of the Western European Variscan chain has only been the subject of very few recent studies (Link *et al.*, 2019; Cugerone *et al.*, 2020). This consideration is particularly true for tungsten mineralization, but also for gold, which represents the most widespread deposits of interest in the Pyrenees (Poitrenaud, 2018; Poitrenaud *et al.*, 2019).

The most important tungsten deposit in the Pyrenees and one of the largest European deposits is the Salau mine in the Central Pyrenees (Fonteilles *et al.*, 1989). It was the subject of major mining work realized by the Société Minière d'Anglade (SMA) and its scheelite mineralization ($CaWO_4$) produced 13 950 t WO_3 of concentrates between 1970 and 1986. Like all the tungsten occurrences from the Pyrenees, the Salau deposit has been described as a scheelite skarn mineralization (Fonteilles and Machairas, 1968; Derré, 1973; Soler, 1977; Derré *et al.*, 1980; Derré, 1982; Kaelin, 1982; Derré *et al.*, 1984; Lecouffe, 1987; Zahm, 1987; Fonteilles *et al.*, 1988; Krier-Schellen, 1988; Fonteilles *et al.*, 1989; Palau i Ramirez *et al.*, 1995, 1997). The term "skarn" is at the heart of a semantic debate. It derives from the vocabulary of the Swedish miners to designate the iron and magnesium rich silicate matrix of an ore (Jébrak and Marcoux, 2008). The different definitions of the term "skarn" show that this type of mineralization requires two essential conditions: an assemblage of calcic or magnesian silicates (garnet, pyroxene, wollastonite, vesuvianite, olivine, amphiboles, serpentines) and a genesis in relation with a contact metamorphism (Goldschmidt, 1911; Fonteilles and Machairas, 1968; Einaudi *et al.*, 1981; Einaudi and Burt, 1982; Meinert *et al.*, 2005).

It is described that the Salau mineralization was formed during two stages, a prograde stage where metasomatism at the contact with the intrusion transformed carbonate rocks in calcic silicate skarns and a retrograde stage associated with "hydrothermal alteration" where the previously formed skarns are impregnated with massive sulphides (Derré *et al.*, 1980; Fonteilles *et al.*, 1989). Most of the scheelite appears during this retrograde stage (Lecouffe, 1987). During previous mining exploitation, the cut off grade of the ore was 0.8% WO_3 and only the "hydrothermally altered" retrograde skarn (Derré *et al.*, 1980; Fonteilles *et al.*, 1989), with abundant scheelite, was exploited. The exploitation of the deposit changed dramatically in the last few years of production, when mining was focused on a very rich ore type, with an average grade of 1.5% WO_3. Gold has also been found in significant grades (5–10 g/t). Despite still significant proven resources, the mine was closed in 1986, due to the drop of tungsten prices. In comparison with other skarn mineralizations, the Salau deposit shows exceptional tungsten contents, among the highest in the world (Derré *et al.*, 1980; Fonteilles *et al.*, 1988). The existence of gold in tungsten mineralization, also with high grade, is a rare phenomenon in most other deposits of the same type (Meinert *et al.*, 2005) and raises the question of the superposition of mineralizing events.

Recently, a U/Pb dating study was performed to provide time constraints on the genesis of the Salau deposit and to understand the setting of this complex mineralization (Poitrenaud *et al.*, 2019). U/Pb datings performed on zircon, apatite and scheelite show that the granodioritic intrusion and the mineralization associated with the skarn are contemporary at 295 ± 2 Ma, while the massive sulphides and gold ore was formed later, at 289 ± 2 Ma suggesting the superposition of two mineralizing events.

In this study, and in order to complement the geochronological data recently acquired, we bring new observations and constraints for the tungsten mineralization genesis combining field survey, 3D modeling, mineralogy, microchemistry and isotopic geochemistry, at the scale of the orebodies. It appears that contrary to what was described by several authors as a simple skarn (Derré *et al.*, 1984; Lecouffe, 1987; Fonteilles *et al.*, 1989), the Salau deposit corresponds to the superposition of a vein breccia with massive sulphides (pyrrhotite and chalcopyrite dominant), coarse-grained scheelite and gold located in ductile-brittle shear zones intersecting a calcic silicate skarn, with rare scheelite and disseminated sulphides. The metallogenic implications of these results are discussed by repositioning the deposit in the regional late Variscan geodynamic, magmatic and hydrothermal context of the Pyrenees area.

2 Geological context

2.1 Regional geology

The Axial Zone of the Pyrenees was affected by the Variscan orogeny between 330 and 290 Ma. This zone consists essentially of Precambrian to Paleozoic metasediments intruded by numerous late Variscan granitic plutons characterizing the suprastructure, and of vast gneiss and migmatites domes forming the infrastructure (Denèle *et al.*, 2014; Fig. 1a). The Variscan deformation seems to relate to a single event during which the Axial Zone is characterized by a strong structural contrast between the suprastructure and the infrastructure. Indeed, the suprastructure mainly records a NS shortening in upper to medium crust, and the roof of the infrastructure outcropping in HT metamorphic domes, was exhumed in a context of EW stretching (de Sitter and Zwart, 1960; Zwart, 1979; Carreras and Capellà, 1994; Cochelin *et al.*, 2018). Recent studies suggest that the deformation of these two domains appears to be largely synchronous in a dextral transpressive regime (Gleizes *et al.*, 1998b; Mezger, 2009; Denèle *et al.*, 2014; Cochelin, 2016; Cochelin *et al.*, 2018). This episode is associated with a dominant calc-alkaline magmatism and the intrusion of numerous plutons, mainly of

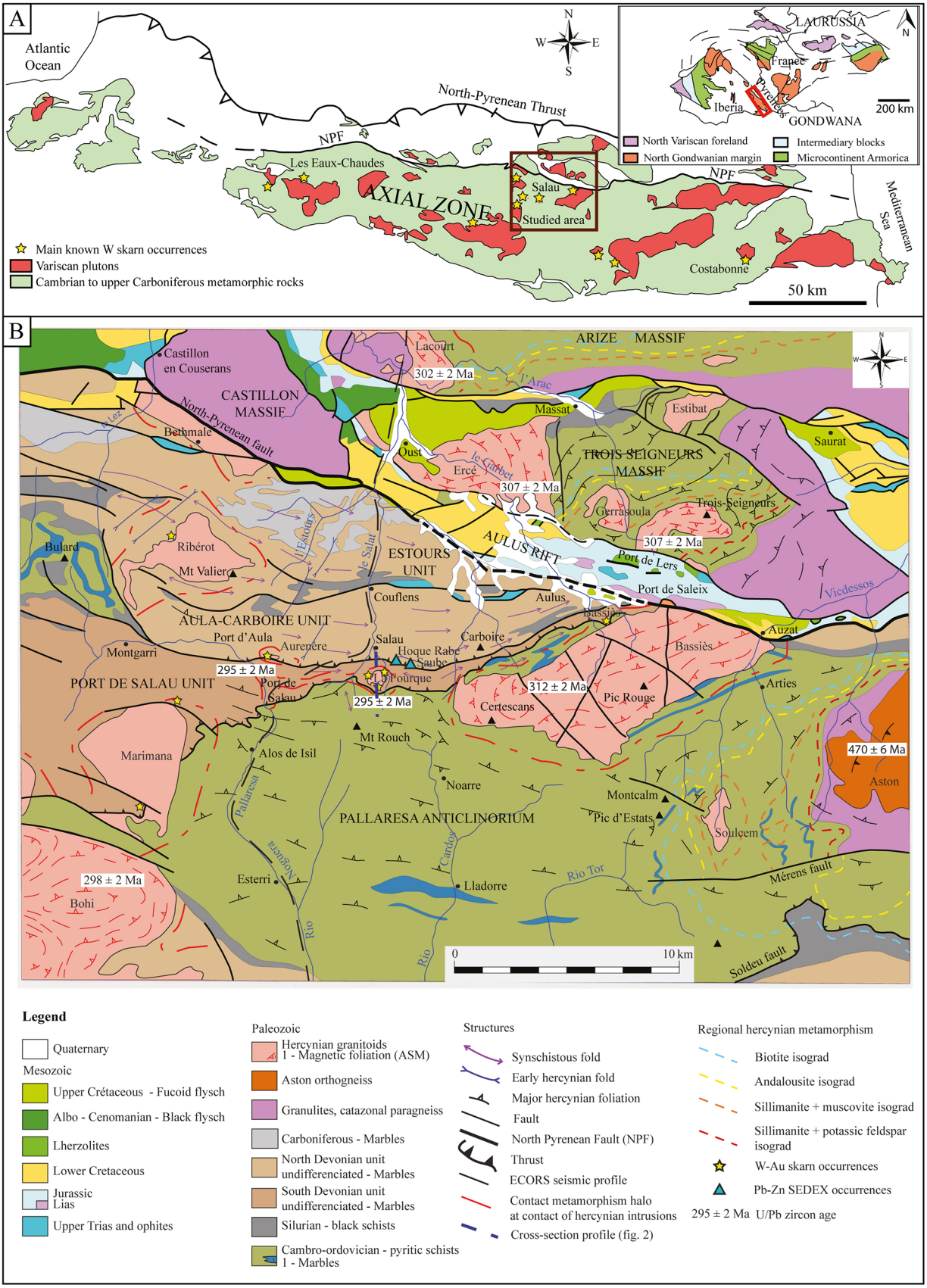

Fig. 1. (a) Simplified geological map of the Paleozoic domain of the Pyrenees (France) modified according to Denèle *et al.* (2011); (b) Regional structural diagram of the Salau zone modified according to Colchen *et al.* (1997).

Fig. 1. *(a) Carte géologique simplifiée du domaine Paléozoïque des Pyrénées (France) modifié d'après Denèle* et al. *(2011) ; (b) Schéma structural régional de la zone de Salau modifié d'après Colchen* et al. *(1997).*

granodioritic type (Debon and Guitard, 1996; Denèle *et al.*, 2014).

The central part of the Axial Zone is structured by several plurikilometric shear zones, generally considered of Variscan age and possibly reactivated during the Pyrenean collision (Fig. 1a) (McCaig and Miller, 1986; Barnolas and Chiron, 1996). However, there is no consensus about the age and the relative importance of the reactivation of these different shear zones, in particular due to the scarcity of post Variscan stratigraphic markers (Cochelin *et al.*, 2018). Synkinematic white micas of some ductile shear zones have been dated between the Eocene and Jurassic by the $^{40}Ar/^{39}Ar$ method (McCaig and Miller, 1986; Monié *et al.*, 1994; Wayne and McCaig, 1998; Vissers *et al.*, 2017); their ages suggesting both a mica neoformation during Pyrenean or even Mesozoic tectonometamophic episodes but also possibly a partial reopening of the K/Ar system of inherited Variscan minerals. However, the $^{40}Ar/^{39}Ar$ ages obtained on mica cannot be used with confidence to determine the age of these faults. On one hand, the closing temperature of the $^{40}Ar/^{39}Ar$ system in mica is between 300 and 425 °C (Harrison *et al.*, 1985, 2009; Villa, 1998; Cassata *et al.*, 2009). On the other hand, the Mesozoic ages obtained in these shear zones show a partial to total rejuvenation of the isotopic systems linked to metasomatic events (250–550 °C) of Permian to Cretaceous age (Boulvais *et al.*, 2007; Poujol *et al.*, 2010; Fallourd *et al.*, 2014; Boutin *et al.*, 2016). This problem about the age rejuvenation of synkinematic mica has been raised in particular in the plutons of Maladeta, Néouvielle and Canigou (Jolivet *et al.*, 2007; Maurel *et al.*, 2008; Metcalf *et al.*, 2009). On the Salau deposit, a U/Pb age on apatite of 289 ± 2 Ma was recently obtained on one of these shear zones known as the Veronique fault, where most of the sulphide mineralization is hosted (Poitrenaud *et al.*, 2019).

Late Variscan magmatism in the Pyrenees is represented by approximatively thirty plutons, mainly of calc-alkaline nature, distributed over the whole Axial Zone (Autran *et al.*, 1970; Barnolas and Chiron, 1996). The magnetic structures of these plutons are consistent with their synkinematic emplacement during a D2b dextral transpressive episode (Evans *et al.*, 1997; Gleizes *et al.*, 1998b, 2001, 2006; Auréjac *et al.*, 2004; Denèle *et al.*, 2014). A close relationship between the activation of shear zones and pluton emplacement is proposed as an ascent mechanism of magma in the crust (Denèle *et al.*, 2008). U/Pb ages on zircon dates the emplacement of most of these plutons from the Upper Carboniferous to the Lower Permian (Romer and Soler 1995; Paquette et al., 1997; Roberts *et al.*, 2000; Maurel et al., 2008; Olivier *et al.*, 2008; Aguilar *et al.*, 2013). Most of the late Variscan plutonic massifs of the Pyrenees show a wide compositional variation, with a mafic external part (gabbros, diorites, granodiorite), while their core typically consist of monzogranites (Barnolas and Chiron, 1996). All of these facies are then cross cut by small leucogranitic bodies, as dyke swarms (Paquette *et al.*, 1997; Metcalf *et al.*, 2009). These granitoids, with an increasing differentiation, are emplaced according to several pulses, during a short period of a few My (Gleizes *et al.*, 2006).

A single crustal thickening subdivided into 3 phases, is proposed for the Variscan segment of the Pyrenees (Denèle *et al.*, 2009a, 2014; Laumonier *et al.*, 2010). The early D1 phase is characterized by crustal thickening during an episode of N-S to NE-SW shortening in the upper and middle crust with thrusts and folds development. This phase is possibly associated with a low to medium degree Barrovian metamorphism. According to these authors, it induces the development of a penetrative major schistosity in the middle crustal levels. A D2a syn-convergence phase of crustal scale lateral flow of the lower crust with an EW to NW-SE stretching direction, contemporary with the metamorphic peak of HT/LP reaching partial melting (Deloule *et al.*, 2002; Maurel *et al.*, 2008). A D2b crustal-scale folding phase leading to the formation of tight sub-vertical, multi-scale, south-verging E-W folds in the upper crust and open, kilometer-wide folds in the middle crust. The open folds of more competent Ordovician laccoliths in the middle crust led to the formation of gneissic domes (Denèle *et al.*, 2007, 2009b). The intrusion of calc-alkaline plutons is considered contemporaneous with this dextral transpressive event (Bouchez and Gleizes, 1995; Evans *et al.*, 1997; Gleizes *et al.*, 1998a). The last phase of deformation D3 corresponds to the localization of the deformation during the cooling of the Variscan crust in a still NS to NE-SW general shortening context leading to the formation of EW to NW-SE multi-kilometric shear zones with a dextral reverse kinematic (Mezger *et al.*, 2012; Van den Eeckhout and de Bresser, 2014).

2.2 The Salau deposit

The Salau sector, located on the northern flank of the Pallaresa anticlinorium, within Paleozoic metasediments, is bordered to the south by the Ordovician terranes of the Pallaresa zone and to the north by the North-Pyrenean fault (Fig. 1b; Colchen *et al.*, 1997). This fault separates the Paleozoic terranes of the axial zone with the Mesozoic Aulus rift. The Salau deposit is hosted in a limestone and shale formation of the Lower Devonian known as the Port of Salau formation, with south verging recumbent folds (Bodin and Ledru, 1986). This unit is intruded by late Variscan calc-alkaline granitoids (*e.g.* Marimaña, Bassiès or La Fourque; Fig. 1b). These plutons developed contact metamorphic aureoles associated with scheelite skarn mineralization such as Salau (Derré, 1982).

The Salau deposit is located at the contact between the small granodioritic massif of La Fourque and carbonate metasedimentary formations of Devonian age (Fig. 2). La Fourque massif includes two main intrusive facies, the apical La Fourque granodiorite on the periphery, and a porphyroid monzogranite in the core of the massif. The apical granodiorite is predominantly gray in color, with a fine-grained equigranular texture (0.5–1 mm) and forms an external halo 100 to 250 m wide, surrounding the monzogranitic core. It consists essentially of interstitial xenomorphic quartz, zoned plagioclase feldspar, sparse microcline, abundant biotite and rare zircon and apatite (Soler, 1977). This apical granodiorite thins and disappears at depth. In underground mining works, porphyroid granodiorite is the dominant facies. This facies contains microcline crystals (20%) up to 1 cm in length. Geochemical studies of Guy (1979), Raimbault (1981) and Toulhoat (1982), demonstrated the chemical composition differences between these 2 petrographic facies.

The lithological interface between Devonian marbles and the plutonic rocks is partly reactivated by shear zones, the main

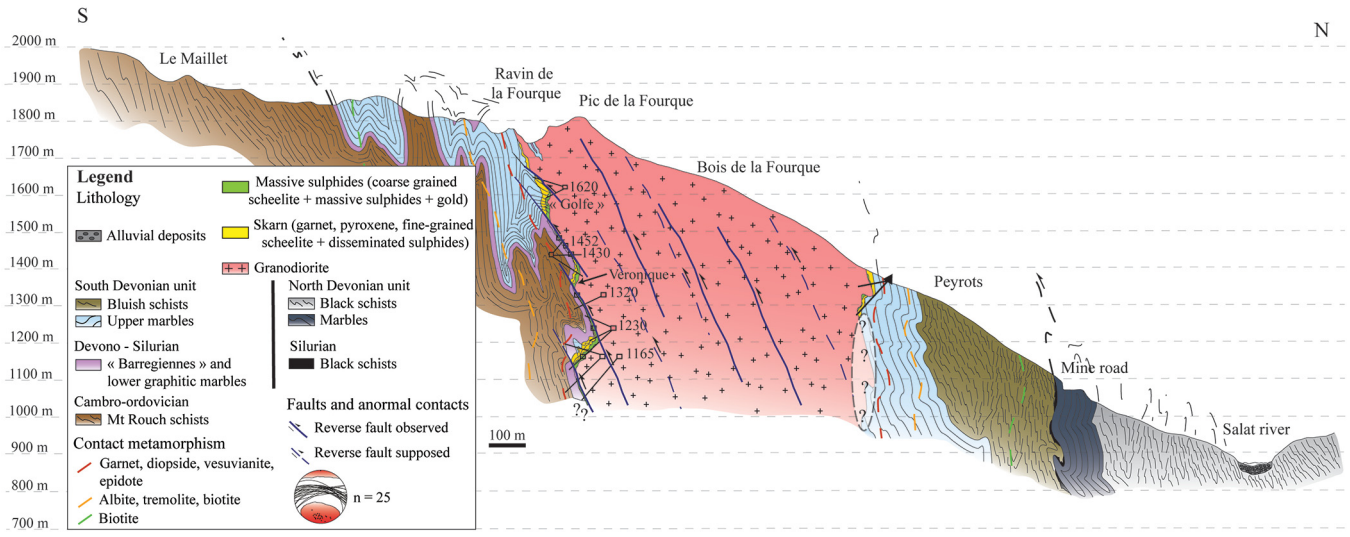

Fig. 2. N-S section of the Fourque massif established from field observations and historical drilling data. The location of the samples studied is shown in blue. The contact metamorphism isograds intersect the regional folds that precede the establishment of the Fourque intrusion in a large-scale antiform. The massive sulphide ore is located along the Véronique fault on the southern contact of the granodiorite. Later, late faults E-W 70°N move the ore more than 100 in a reverse movement.

Fig. 2. *Coupe N-S du massif de la Fourque réalisée à partir des observations de terrain et des données de sondages historiques. La localisation des échantillons étudiés est reportée en bleu. Les isogrades de métamorphisme de contact recoupent les plis régionaux qui précèdent la mise en place de l'intrusion de la Fourque dans un antiforme à grande échelle. Le minerai à sulfures massifs est localisé le long de la faille Véronique sur le contact sud de la granodiorite. Postérieurement, des failles tardives E-W 70°N déplacent le minerai de plus de 100 selon un mouvement inverse.*

one is the Veronique fault, emplaced at the southern boundary of the La Fourque pluton (Lecouffe, 1987). The emplacement of La Fourque pluton initiated important metasomatic reactions at its contact. A calcic silicate skarn with scheelite mineralization (grossular, hedenbergite) was developed. The particularity of the ore mined at Salau is its high content in sulphides, in particular of massive pyrrhotite (Derré *et al.*, 1980). According to Derré *et al.* (1984), the origin of the massive sulphides in the ore is linked to the circulation of hydrothermal fluids rich in tungsten, gold and copper during the retrograde stage of contact metamorphism. According to Fonteilles *et al.* (1989); this "hydrothermal alteration" reacted at high temperature with the previously metasomatized carbonate host rocks during the prograde stage. This episode precipitates a mineralization rich in scheelite, pyrrhotite and chalcopyrite. These authors interpreted the source of this "hydrothermal alteration" as linked to the formation of skarns and therefore to La Fourque granodiorite. Considering crosscuting relationships between La Fourque pluton and the shear zones, other authors (Ledru, 1986; Ledru and Autran, 1987), attributed the precipitation of late abundant sulphides to the development of the shear zones. These authors also proposed a different source of the fluids from that of La Fourque granodioritic pluton. These hypotheses were recently confirmed by the study of Poitrenaud *et al.* (2019), which shows that there is a telescoping of two mineralization types. The activation of the shear zones was initiated ca. 6 My after the emplacement of La Fourque pluton in the metasedimentary series and the development of the calcic silicate skarn. Other similar mineralizations to the Salau deposit have been described across the axial zone of the Pyrenees (Derré *et al.*, 1984). The location of the Aurenère skarn occurrence at the west of Salau (Palau i Ramirez *et al.*, 1997) and Bassiès skarn occurrence (Colchen *et al.*, 1997; Poitrenaud, 2018) at the east of Salau, from which some samples were collected for comparison with the results of this study have been reported in Figure 1b. In addition, a few samples were also collected, for comparison, on the Pb-Zn SEDEX mineralization of Saube and Hoque Rabe, located east of Salau (Derré *et al.*, 1980; Pouit, 1984; Fig. 1b).

3 Description of the different types of orebodies

The Salau deposit was mined from two main ore bodies, the Bois d'Anglade and the Véronique sectors. The Bois dAnglade is located at the south-east of La Fourque pluton.

3.1 The Bois d'Anglade sector

The mineralized occurrences of the Bois d'Anglade sector are located in an embayment of the granodioritic massif (Derré *et al.*, 1980) in the carbonate metasediments (Fig. 2). The host rocks are structured in a sub-vertical N110°E trending antiform. Most of the Bois d'Anglade mineralization is located to the east and to the west of a sub-outcropping granodiorite stock, cross cut by a of N120°E 80°N shear zones system. Exoskarns (0–30 m thickness) are developed in carbonate metasediments along the contact with the intrusion.

Endoskarns are also observed at the contact with the pluton, in a relatively thin zone (< 50 cm). At the surface, the Bois d'Anglade area corresponds to an open pit of more than 50 m in height, mined by the Société Minière d'Anglade (SMA). It consists of three main levels that allow to observe the contact between the granodiorite and the host rock. The Veronique fault cannot be observed directly from the open pit, however, a few developments oriented to the south allow to identify figures of intense deformation. For example, on some outcrops in the southern part of the open pit, the granodiorite is strongly altered (silicified and invaded with massive sulphides) and fracturated according to networks of EW brittle faults steeply dipping towards the north. Moreover, on this same wall, exoskarns in contact with the intrusion are generally rich in massive sulphides (dominant pyrrhotite, but also arsenopyrite, chalcopyrite and sphalerite). The eastern part of this open pit does not show sheared granodiorite but the skarns are rich in massive sulphides. The northern part shows an undeformed contact and the skarn is not rich in massive sulphides (Fig. 3a). Accordingly, the presence of these massive sulphides seems to be strongly correlated with the deformation observed. The surrounding area mainly consists of marble with a sub-vertical N100°E stratification. At contact with the host rocks, the granodiorite is altered in endoskarn which frequently shows massive epidotization in parallel bands of few decimeters. Scheelite and pyrrhotite are rare.

In the Bois d'Anglade area, exoskarns are generally poor in scheelite and pyrrhotite (Fig. 3a). They consist of monomineral ribbons, generally dominated by pyroxenes (hedenbergite or diopside) or by the decimetric alternation of ribbons rich in pyroxene, epidote and titanite (light skarns), and of garnet, pyroxene and epidote ribbons (dark skarns). Skarns are locally cross cut by quartz, calcite and chlorite veins precipitated in tension jogs near shear zones in the granodiorite. Scheelite is commonly concentrated in the hedenbergite zone of exoskarn (Fig. 3a), but can also be found at the border of the endoskarn. It is generally fine (< 100–200 μm) and forms ribbons in the bedding of metasomatized marbles. When the skarns have a low content in sulphides (disseminated), the scheelite is fine and also disseminated.

3.2 The Veronique fault

In underground mining works, the Véronique fault is mainly outcropping close to the orebodies of the Véronique district, at the south of La Fourque pluton. The fault has a N120°E average strike with variable dip towards the north (40°N to 80°N). The orebodies have a relatively irregular morphology and distribution in several lenses, from 1490 m to 1080 m in the area explored by mining works and drilling. The ore mined by the SMA in these orebodies had the particularity of containing very high scheelite average contents (> 1.5% WO_3) sometimes reaching locally more than 20% WO_3 (Poitrenaud, 2018). In the Véronique district, important gold anomalies were discovered with contents of 5 to 10 g/t Au (Fonteilles *et al.*, 1989) with analyzes up to 16 g/t Au. Mineralization mainly occurs as, steeply dipping to the north, lenses of massive sulphides with coarse-grained scheelite hosted in skarns, marbles or in altered and mylonitized granodiorite (Figs. 3b and 3c). The surrounding granodiorite close to these lenses is laminated, silicified and contains scheelite and arsenopyrite veins (Fig. 3g).

The dextral reverse movement of the shear zone has been determined with sigmoid-shape microlithons between shear zones in the granodiorite and in the skarns intersected by the Veronique fault (Figs. 3e and 3f). Folds show the posteriority of this massive sulphides-bearing fault compared to the calcic silicate skarns (Fig. 3c). The extension of the mineralized bodies at the footwall of the Veronique fault, intersected by drilling to the northwest down-dip extension, show a reverse dextral pluri-hectometric shift between two skarn compartments, which is in agreement with observations realized by Lecouffe (1987). In La Fourque granodiorite, close to openings along faults or in breccias, subhorizontal quartz, calcite, adularia, pyrrhotite and powdery chlorite veins precipitated in tension jogs highlights the reverse movement of the Veronique fault.

The ore from the Veronique fault has a breccia texture (Fig. 3b) composed of host rock elements (shreds of intensely folded graphitic marbles, skarns, blocks of altered mylonitic granodiorite) cemented by massive pyrrhotite and coarse-grained scheelite (100 μm–1 cm). Shear zones at contact with the Veronique fault are represented by a several meter thick band in the pluton and the host rocks. Decimetric to metric veins of laminated white quartz are commonly found in contact with granodiorite (Fig. 3c). Massive sulphides and coarse-grained scheelite are discordant on the skarns, which remain as relics (Fig. 3b). Massive pyrrhotite locally occur as a stockwork in the skarn. Quartz and calcite are in the interstices between large and ovoid scheelite crystals (> 200 μm). This assemblage is also found in endoskarns and in fractures of altered granodiorite (quartz, muscovite, epidote, calcite).

The Veronique fault has also been observed far from the La Fourque pluton, in the area of the Plagnau long ravine (1 km to the west of the deposit) and in the Pallaresa valley (10 km to the west of the deposit). In the first case, it is located at the interface between the Ordovician shales (Mont Rouch formation; Fig. 1b) and the Devonian marbles (Salau marble formation; Fig. 1b) and is marked by a 3m thick EW fault breccia steeply dipping to the north. The breccia consists of schist shreds or multi-metric marble blocks and is cemented by a fine quartz and clay matrix. The breccia is also rich in pyrite, often as decimetric lenses. At surface, the drags of parallel satellite faults close to the breccia are consistent with a dextral kinematic in the N100°E 85°S schistosity of the Ordovician schists. Despite the presence of this fault, which appears to be the lateral extension of the Veronique fault, no massive sulphide and scheelite mineralization has been observed. In the Pallaresa valley, the fault intersects the Ordovician schists along a N110°E 85°S orientation. The fault zone is marked by several veins of white quartz, rich in pyrite, separating several schist compartments, sheared and brecciated by a dextral reverse movement. Analyzes on areas rich in pyrite did not show significant gold (< 0.1 g/t) or tungsten contents (< 0.01% WO_3).

3.3 Relationships between mineralizations and magmatic rocks

The R1 cuddy of the Salau mine at level 1230 (Quer de l'Aigle; Lecouffe, 1987) shows boudins of dark diorite enclaves

in La Fourque granodiorite and late aplitic dykes, which cross cut both La Fourque granodiorite and these dioritic enclaves. Aplite dykes are frequent at the base of the Salau deposit and near the Veronique fault where they outcrop as swarms. A cluster of coarse-grained scheelite and massive sulphide ore occurs at the border of an aplitic stockwork hosted by a granodioritic breccia (Fig. 3d). Aplite mainly consists of quartz and feldspar, with epidote alteration. Its contact with massive sulphides, marked by a border poor in feldspar and rich in quartz, is progressive and well zoned, showing their contemporaneity, with multi-millimeter ribbons of sphalerite at contact with the dyke, then galena and finally pyrrhotite and massive chalcopyrite (Fig. 3d).

Near the Veronique fault, centimetric veins of black quartz and tourmaline cross cut La Fourque granodiorite (Fig. 3h) in which they constitute a network of parallel veins resulting in a ribboned texture. They also outcrop locally as decimetric veins near the aplitic veins of the R1 cuddy at level 1230. These veins are grouped into two sub-orthogonal populations with relatively constant orientations (N80E 45°N and N170E 70°S). The tourmaline veins are parallel to the Veronique fault when they are in its surroundings. At contact with these veins, the granodiorite is silicified, exempt of biotite, and altered in a quartz, muscovite and titanite greisen (Fig. 3h). Arsenopyrite and more rarely wolframite (Lecouffe, 1987) are neoformed in silicified granodiorite (Fig. 3g) with small discordant calcite and pyrrhotite veins. Tourmaline veins evolve laterally towards the massive sulphide ore lenses of the Veronique fault.

4 3D modeling

To constrain the orebodies geometry at the deposit scale and the spatial relationships between skarn and massive sulphides, a 3D model of the mineralizations was constructed using the software Micromine ^{TM} (Fig. 4a). The data set used was extracted from logs of diamond and destructive drill holes realized during historical exploration and exploitation of the Salau deposit (Guiraudie *et al.*, 1964; Passaqui and Costargent, 1965; Prouhet *et al.*, 1966; Michard and Bouquet, 1986; internal SMA archives). In total, 677 logs of diamond drilling, 14 logs of destructive drilling and 141 air-blast holes from BRGM and SMA were collected (Fig. 4a). In addition to this drilling information, data from 2373 samples collected along exploitation faces were digitized. The length of the diamond drills varies from 25 to 492 m. Most of the analysis data relate to tungsten, expressed in % WO_3. Only a hundred analyzes provide informations for gold and silver contents. Most of the high tungsten contents are located in the surroundings of the Veronique fault. Their use, combined with harmonized lithological logs, gives an indication of the geological structure of the deposit, which seems complex, in particular for the correlation between neighbouring drillholes. This is explained by the very irregular morphology between the granodioritic intrusion and the host rocks. 3D modeling of the mineralization geometry, required the realization of numerous serial sections to best constrain their extent.

The Veronique fault connects the Veronique district and the Bois d'Anglade, as observed in the field. To the east of the deposit, the fault cross cuts the Quer de l'Aigle area where a breccia-type mineralization with massive sulphides is outcropping. In this zone, the granodiorite has a very irregular contact with the host rocks, which explains the numerous embayments with skarn mineralization. The fault extends eastward under the Quer de l'Aigle massif. A E-W trending satellite fault crosscutting by the granodiorite was identified 50 m to the north of the Veronique fault. This satellite fault is also mineralized in massive sulphides and coarse-grained scheelite, but with a restricted thickness of 0.50 m to 1 m. At the scale of the deposit, the 3D model allows to visualize the shift generated by the fault between the orebodies of the Veronique district (Figs. 4b and 4c). The two skarn compartments identified by mining work and drilling are shifted with a dextral reverse movement of more than 250 m on each side of the Veronique fault. The fault has an average N100°E 70°N direction and is represented by a breccia cemented with massive sulphides and coarse-grained scheelite at the contact between granodiorite and host rocks.

5 Paragenetic synthesis

The mineralogical assemblages of the Salau deposit are complex due to the spatial and temporal superposition of two distinct mineralizations. Observation of more than 250 thin and polished sections allow to distinguish the main characteristics for each type of ore (Fig. 5).

The Bois d'Anglade ore type shows a calcic silicate and disseminated scheelite skarn, hosted by Devonian marbles. The prograde stage consists of a grossular, hedenbergite and diopside assemblage and the retrograde stage of a wollastonite, vesuvianite and fine scheelite assemblage (Fig. 6a). During retrograde hydroxylation, garnets and pyroxenes are respectively retromorphosed in epidote (clinozoisite) and amphibole (ferroactinote; Fig. 6f). Disseminated sulphides (arsenopyrite, pyrrhotite) filled the grain boundaries of calcic silicates (Fig. 6b). Crystallization of sulphides show the end of the retrograde stage.

The ore from the Veronique fault is a vein breccia which cross cuts granodiorite, skarns and marbles. Black quartz and tourmaline veins are also discordant on the granodiorite. They develop a greisen-type alteration and are locally associated with arsenopyrite. An assemblage of abundant coarse-grained scheelite and massive sulphides with dominant pyrrhotite, chalcopyrite, sphalerite, galena, electrum, native bismuth, laitakarite, native silver (Figs. 6c, 6d and 6e) systematically takes place close to N100°E 70°N fault zones (see Fig. 3c). These sulphides constitute the cement of clasts from adjacent rocks (granodiorite, marbles, calcic hornfels, skarn, skarnoids). Numerous euhedral hydrothermal apatite are associated with these massive sulphides ore. The composition of the sulphide assemblage varies from place to place and is correlated to the nature of the host rock. Graphitic levels are the richest in electrum. Quartz, chlorite and calcite sub-vertical tension jogs mark the vertical stretch induced by the reverse movement of the Veronique fault near the massive sulphide mineralization. Late assemblages with adularia, titanite, laumontite and apophyllite have also been observed, mostly in geodes.

6 Thermobarometric constraints

To estimate the temperature and pressure conditions during the emplacement of the La Fourque granodiorite, microprobe

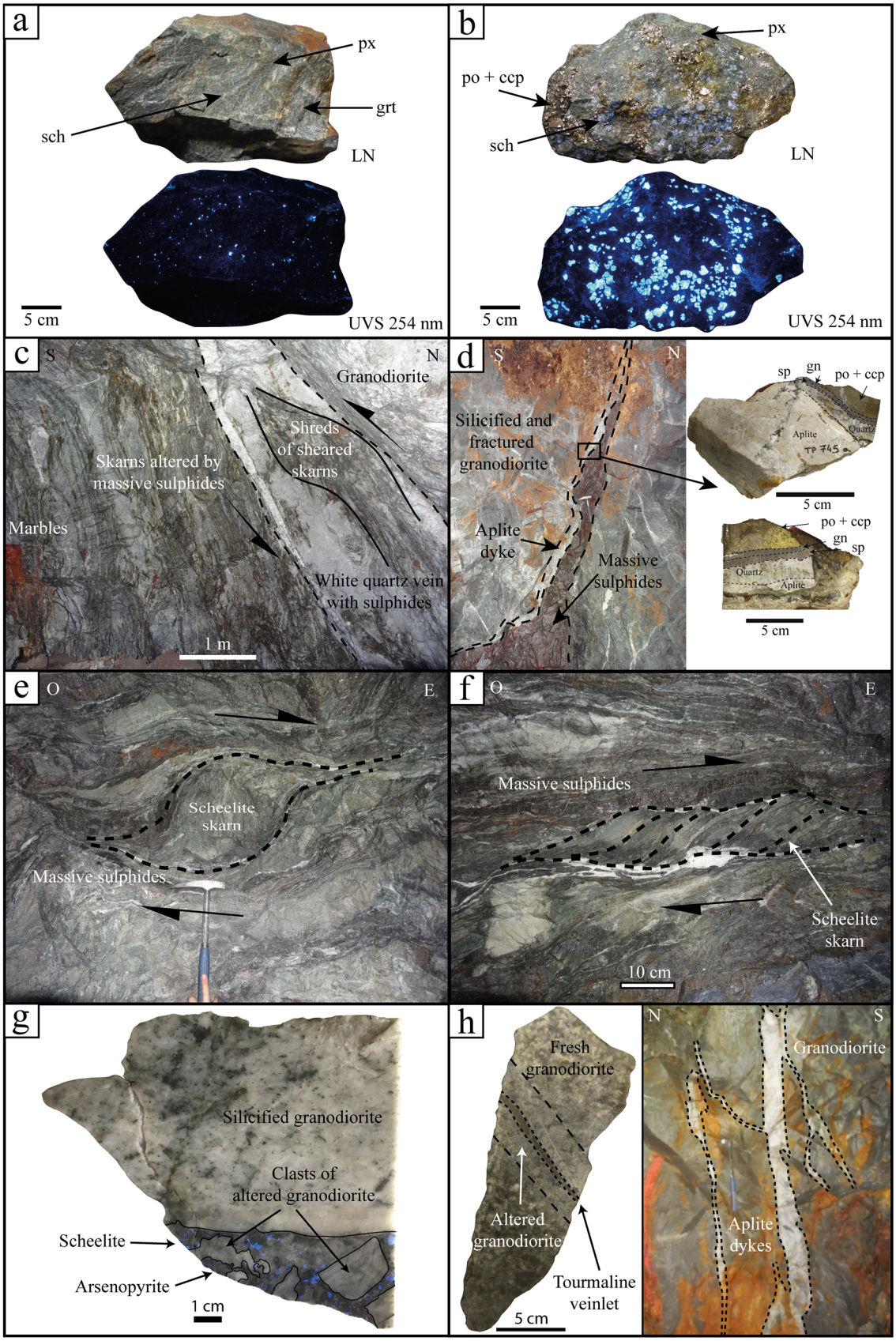
a
px
grt
sch
LN
5 cm
UVS 254 nm
b
px
po + ccp
sch
LN
5 cm
UVS 254 nm
c
S
N
Granodiorite
Shreds of sheared skarns
Skarns altered by massive sulphides
Marbles
White quartz vein with sulphides
1 m
d
S
N
Silicified and fractured granodiorite
Aplite dyke
Massive sulphides
sp
gn
po + ccp
Aplite
Quartz
5 cm
po + ccp
gn
sp
Quartz
Aplite
5 cm
e
O
E
Scheelite skarn
Massive sulphides
f
O
E
Massive sulphides
Scheelite skarn
10 cm
g
Silicified granodiorite
Clasts of altered granodiorite
Scheelite
Arsenopyrite
1 cm
h
Fresh granodiorite
Altered granodiorite
Tourmaline veinlet
5 cm
N
S
Granodiorite
Aplite dykes

Fig. 3. Field photographs showing the following elements: (a) Sample of calcium silicate skarn (garnet, pyroxene), fine scheelite and disseminated pyrrhotite taken from the unstacking of Bois d'Anglade, in natural light and in UVC light 254 nm; (b) Sample of massive sulphide skarn breccia (pyrrhotite, chalcopyrite) and coarse scheelite sampled in the Véronique district at level 1230, in natural light and in UVC 254 nm light; (c) Mine front of the Véronique district at level 1230 showing the ductile-fragile deformation generated by the passage of the Véronique fault at the contact between the Fourque granodiorite and the surrounding Devonian marbles. A vein of white quartz with sulphides underlines the passage of the fault; (d) Aplite dyke intersecting granodiorite at level 1230, accompanied by massive sulphides and coarse scheelite. The macroscopic sample shows the progressive zoning between the aplite dyke and the massive sulphides which underlines their contemporaneity; (e) Photograph of the roof of the Véronique cuddy at level 1243. Sigmoid of skarn sheared along the passage of the Véronique fault showing an East-West direction and a dextral movement; (f) Photograph of the roof of the Véronique cuddy at level 1230. C-S structures in the sheared skarn along the passage of the Véronique fault showing an East-West direction and a dextral movement; (g) Altered granodiorite breccia along the Véronique fault cemented by massive sulphides and coarse scheelite; (h) Fourque granodiorite intersected and altered by tourmaline veins and decimetric aplite dykes which intersect altered granodiorite.

Fig. 3. *Photographies de terrain montrant les éléments suivants : (a) Echantillon de skarn à silicates calciques (grenat, pyroxène), scheelite fine et pyrrhotite disséminée prélevé dans le dépilage du Bois d'Anglade, en lumière naturelle et en lumière UVC 254 nm ; (b) Echantillon de brèche de skarn à sulfures massifs (pyrrhotite, chalcopyrite) et scheelite grossière prélevé dans le quartier Véronique au niveau 1230, en lumière naturelle et en lumière UVC 254 nm ; (c) Front de taille du quartier Véronique au niveau 1230 montrant la déformation ductile-fragile engendré par le passage de la faille Véronique au contact entre la granodiorite de la Fourque et les marbres dévoniens encaissants. Un filon de quartz blanc à sulfures souligne le passage de la faille ; (d) Dyke d'aplite recoupant la granodiorite au niveau 1230, accompagné par un cortège de sulfures massifs et de scheelite grossière. L'échantillon macroscopique montre la zonation progressive entre le dyke d'aplite et les sulfures massifs qui souligne leur contemporanéité ; (e) Photographie de la couronne de la recoupe Véronique au niveau 1243. Sigmoïde de skarn cisaillé le long du passage de la faille Véronique montrant une direction Est-Ouest et un mouvement dextre ; (f) Photographie de la couronne de la recoupe Véronique au niveau 1230. Structures C-S dans le skarn cisaillé le long du passage de la faille Véronique montrant une direction Est-Ouest et un mouvement dextre ; (g) Brèche de granodiorite altérée le long de la faille Véronique cimentée par des sulfures massifs et de la scheelite grossière ; (h) Granodiorite de la Fourque recoupée et altérée par des filonnets à tourmaline et des dykes décimétriques d'aplite qui recoupent la granodiorite altérée.*

analyzes of black and white mica have been performed. All the samples come from La Fourque granodiorite but white mica samples, neoformed from plagioclases, come from E-W shear zones.

Twenty-seven analyzes for black mica were compiled from Lecouffe, 1987 (ESM Tab. 1). The structural formulas were recalculated at 22 oxygen and show that these black micas are biotites, with 55% phlogopite and 45% annite ($K_{0.99}$ $Mg_{1.38}$ $Fe_{1.16}$ $Ti_{0.04}$ $Al_{1.10}$ $Si_{2.90}O_{10}$ $(OH)_{1.85}$ $F_{0.27}$). In these conditions, it is possible to use the geobarometer [P (kbar) = 3.03 × (Al_{tot}) − 6.53] developed by Uchida *et al.* (2007). The range of values in Al_{tot} varies from 3.07 to 3.37 and the range of results obtained varies from 2.75 to 3.63 kbar. The average pressure is around 3.3 kbar, indicating an emplacement depth of La Fourque granodiorite between 10 and 11 km.

The white micas analyzed (4 samples) come from the Veronique district at level 1430 (TP492) and from satellite faults in La Fourque ravine (TP627, TP652a and TP752a; ESM Fig. 1). All analyzes were performed with an ISTO CAMECA SX 100 electronic microprobe, set at 15 kV and 6 nA for silicates. The count time was 10 s for Si, Al, Ti, Fe, Mn, Mg, Ca, Na, K, Cl and F. The structural formulas were recalculated at 22 oxygen and show that these white micas are phengites ($K_{0.94}Na_{0.03}$ $Fe_{0.12}Al_{1.76}Mg_{0.15}$ $Al_{0.80}Si_{3.19}O_{10}$ $(OH)_2$ poor in Fluorine (0.00 to 0.01% F; ESM Tab. 2). The results obtained on biotites and phengites were projected in the thermometric diagram of Monier and Robert (1986) to estimate their crystallization temperatures from Mg and Fe contents (Fig. 7a). Biotites show temperatures above 800 °C. whereas the phengites only reach temperature values between 400 and 500 °C; lower values in agreement with the secondary nature of these white micas, as attested by their structural-textural position. The results on phengites have been projected in the diagram of Massone and Schreyer (1987), to determine a pressure range for the phengite equilibration or minimum pressure if they are as a secondary phase (Fig. 7b). For a range of temperatures between 400 and 500 °C and an average phengitic substitution of Si = 3.2, the phengites of the EW shear zones show minimum formation pressures between 3.2 to 5.9 kbar, so an approximately depth of 10 km.

The composition of amphiboles also allows to estimate the pressure conditions of magma crystallization. Two amphibole analyzes from the La Fourque granodiorite were performed with an electron microprobe by Soler (1977). One analysis was realized on the rim and another on the core of the amphibole (ESM Tab. 3). The structural formulas have been recalculated at 22 oxygen and show that these amphiboles are hornblends ($[Ca_{1.75}$ $Na_{0.19}$ $K_{0.16}]$ $[Mg_{1.95}$ $Fe^{2+}{}_{2.26}$ $Fe^{3+}{}_{0.09}$ $Al_{0.6}]$ $[Si_6$ $Al_{0.66}$ $Si_{1.34}$ $O_{22}]$ $[OH]_2$). In these conditions, it is possible to use several geobarometers on the amphiboles developed by Hammarstrom and Zen (1986), Hollister *et al.* (1987), Johnson and Rutherford (1989), Thomas and Ernst (1990), Schmidt (1992) and Mutch *et al.* (2016). The calibration of Mutch *et al.* (2016) seems to be the most suitable due to the wide range of P-T conditions covered for igneous rocks. The range of values in Al_{tot} varies from 1.26 for the rim to 1.96 for the core of the hornblende and results obtained are respectively of 2.50 and 4.97 kbar (ESM Tab. 3). The pressure estimated at the core of the hornblende at around 4.97 kbar, indicates that the magma started to crystallize around 16–17 km during their ascent in the crust before reaching the emplacement depth of La Fourque granodiorite at 2.5 ± 0.25 kbar (8 to 10 km).

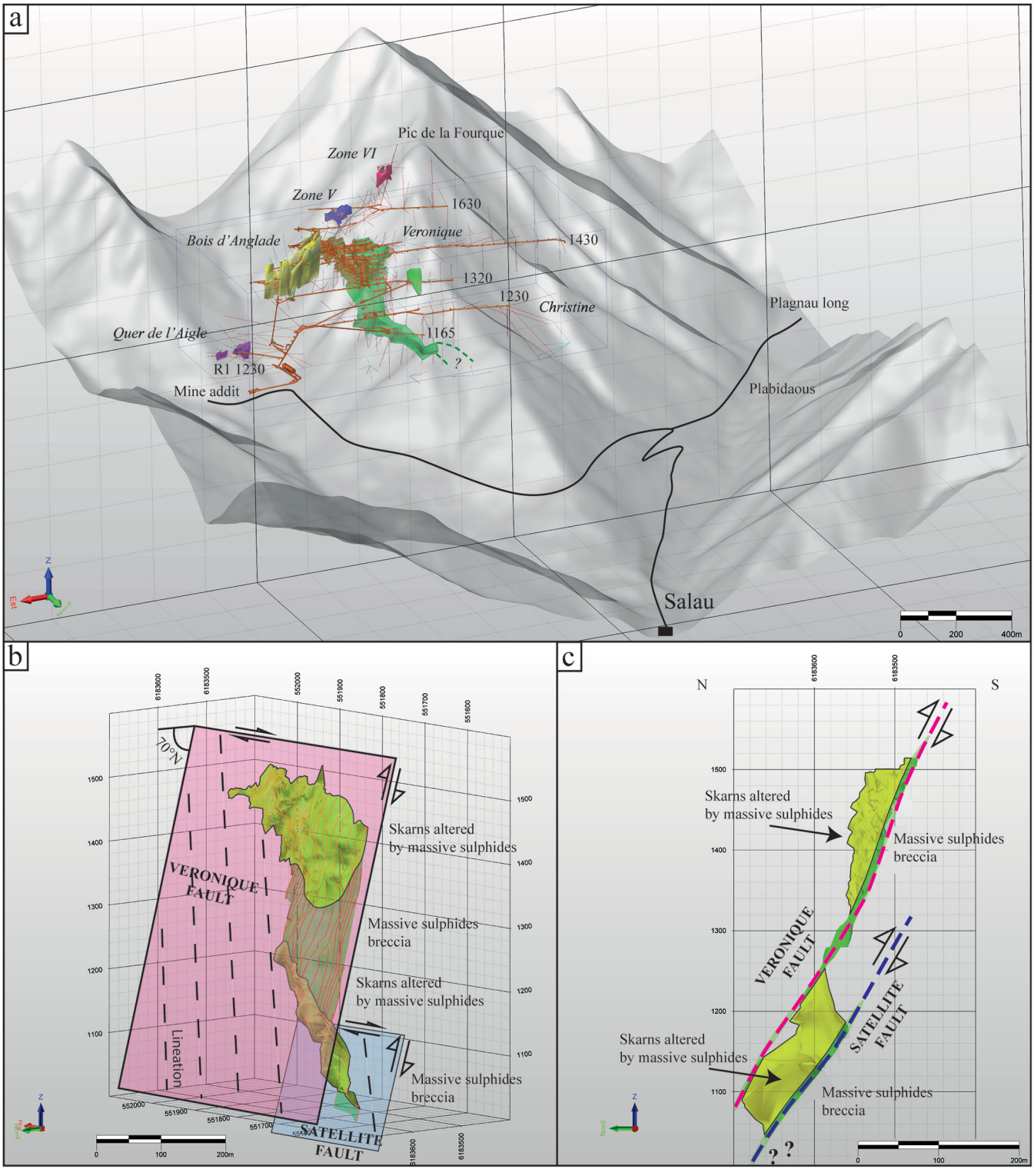

Fig. 4. (a) 3D representation of the different orebodies of the Salau deposit, modelled from SMA and BRGM historical drillhole data; (b) 3D view to the SE of the Veronique district mineralization showing the reverse dextral shift of the two skarn compartments by the Véronique fault; (c) N-S sectional view of mineralization in the Veronique district.

Fig. 4. *(a) Représentation 3D des différents corps minéralisés du gisement de Salau, modélisés d'après les données historiques des sondages de la SMA et du BRGM ; (b) Vue en 3D vers le SE des minéralisations du quartier Véronique montrant le décalage dextre inverse des deux compartiments de skarn par la faille Véronique ; (c) Vue en coupe N-S des minéralisations du quartier Véronique.*

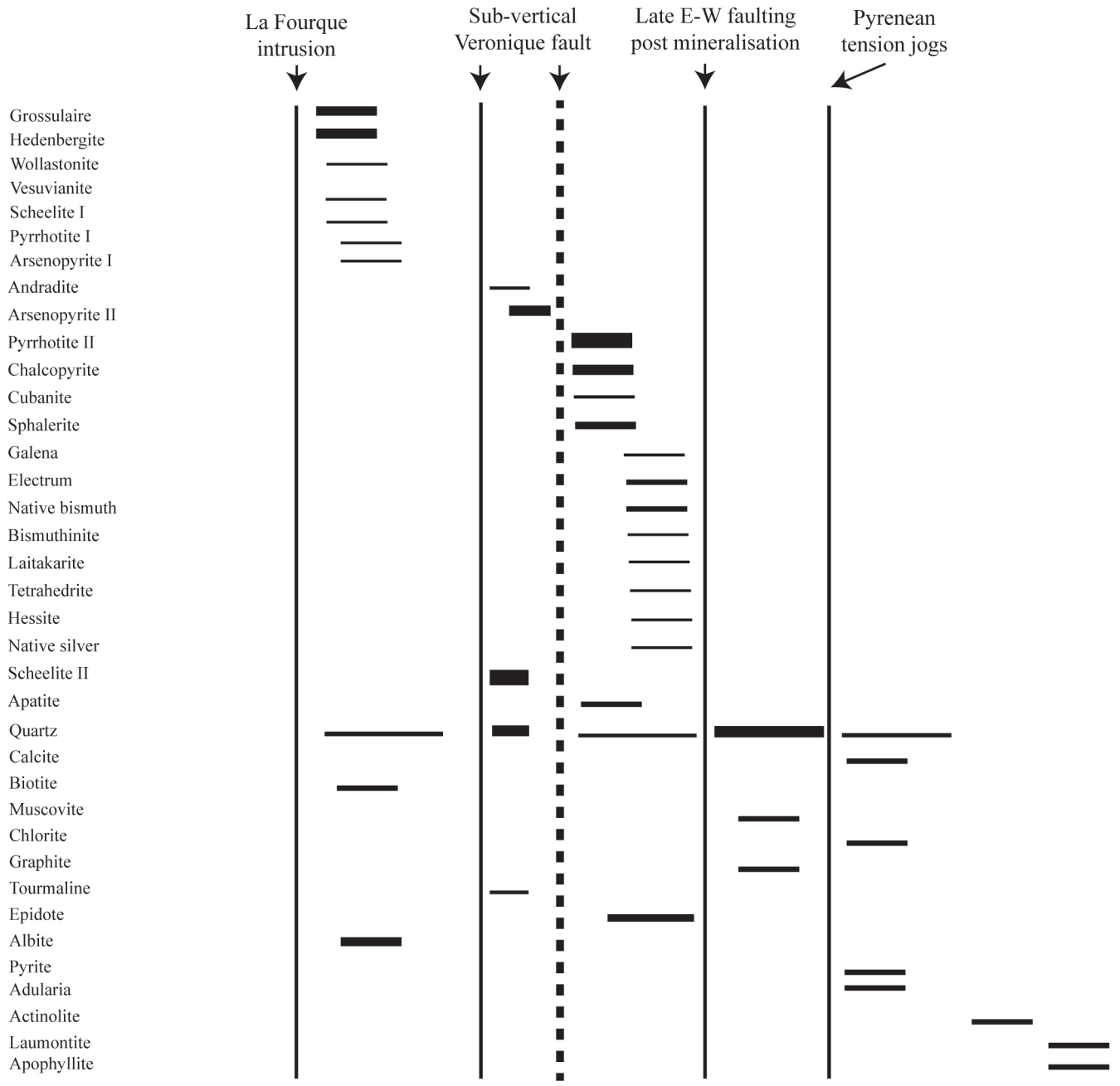

Fig. 5. Paragenetic sequence of the Salau W-Au ore deposit. Three main steps were distinguished, the skarn with scheelite, the breccia with massive sulphides and the late alterations.

Fig. 5. *Séquence paragénétique du gisement à W-Au de Salau. Trois principales étapes ont été distinguées, le skarn à scheelite, la brèche à sulfures massifs et les altérations tardives.*

7 Sulfur isotopes

To determine the sulfur source of the different sulphides in the two ore types (skarn and massive sulphide breccia), sulfur isotopic analyzes were performed in collaboration with the LEHNA laboratory at the Claude Bernard University of Lyon (Tab. 1). For comparison, 5 sulphide samples from the adjacent Aurenère and Bassiès tungsten occurrences as well as Saube and Hoque Rabe lead/zinc occurrences were included in the study (Fig. 1b). 4 samples containing pyrite crystals from different sedimentary formations of the surrounding area were also analyzed to assess their possible role as a source. The various sulphides analyzed (pyrrhotite, arsenopyrite, chalcopyrite, sphalerite, pyrite) were sorted manually under a binocular and approximately 5 g were crushed in an agate mortar to obtain a powder with a particle size of 100 to 300 μm. 16 samples were then analyzed by mass spectrometry (IRMS), online and in continuous flow mode with an elemental

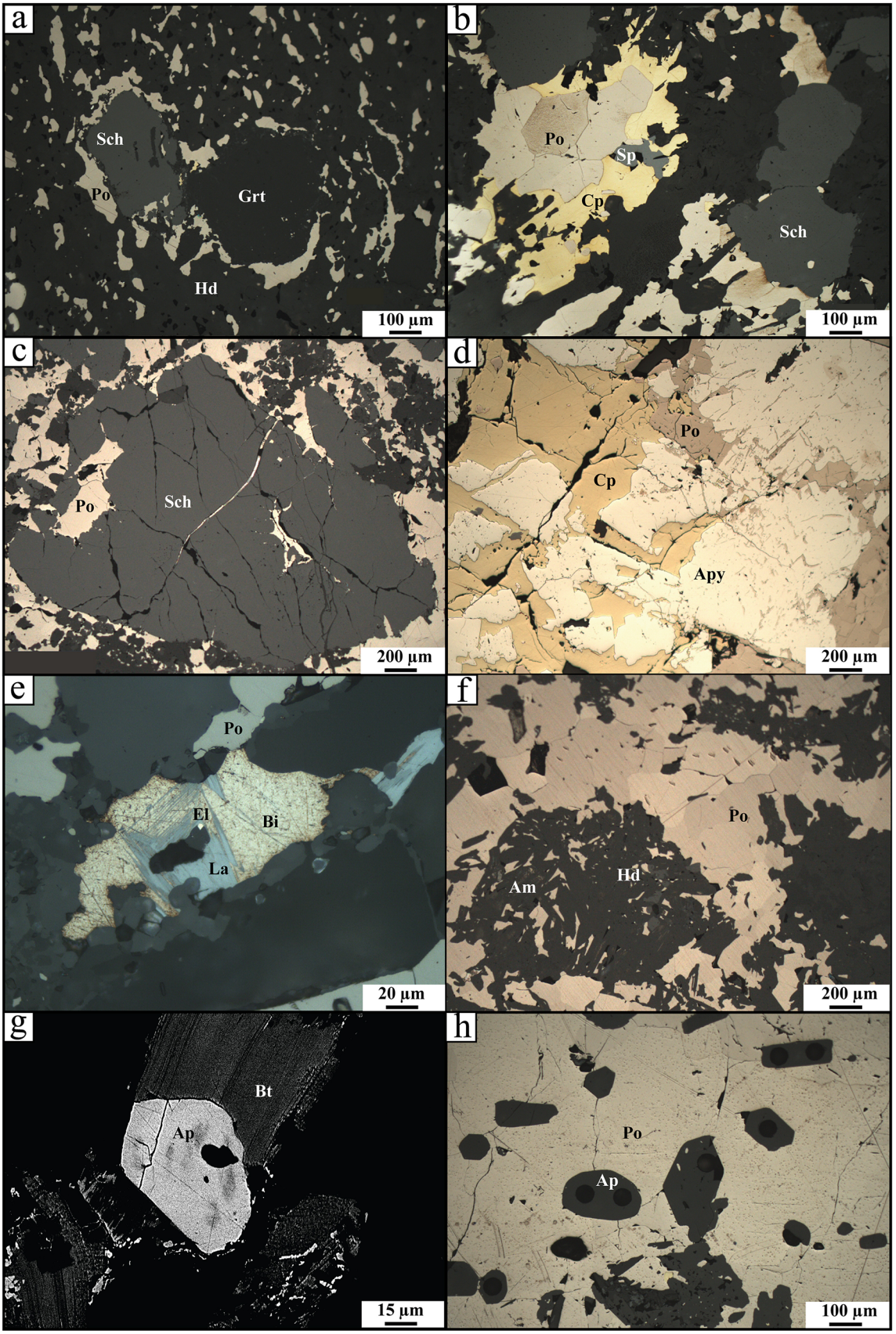
a
Sch
Po
Grt
Hd
100 µm
b
Po
Sp
Cp
Sch
100 µm
c
Po
Sch
200 µm
d
Po
Cp
Apy
200 µm
e
Po
El
Bi
La
20 µm
f
Po
Am
Hd
200 µm
g
Bt
Ap
15 µm
h
Po
Ap
100 µm

Fig. 6. Photographs of polished sections showing the following elements: (a) disseminated pyrrhotite associated with fine scheelite and coarse garnets in the calcium silicate skarn of Bois d'Anglade; (b) massive sulfide paragenesis with a pyrrhotite-chalcopyrite-sphalerite assemblage intersecting the coarse scheelite; (c) coarse scheelite fragmented and cemented by massive pyrrhotite; (d) arsenopyrite crystals fragmented and cemented by chalcopyrite and massive pyrrhotite; (e) native bismuth-laitakarite-electrum assembly typical of the Salau gold paragenesis; (f) hedenbergite retromorphed into an amphibole with intergrowth of pyrrhotite disseminated in the skarns of the Bois d'Anglade; (g) SEM image of a fragmented magmatic apatite contemporary with biotites from the Fourque granodiorite; (h) SEM image of an automorphic hydrothermal apatite contemporary of massive pyrrhotite.

Fig. 6. *Photographies de sections polies montrant les éléments suivants : (a) pyrrhotite disséminée associée avec de la scheelite fine et des grenats grossulaires dans le skarn à silicates calciques du Bois d'Anglade ; (b) paragenèse à sulfures massifs avec un assemblage à pyrrhotite-chalcopyrite-sphalérite recoupant la scheelite grossière ; (c) scheelite grossière fragmentée et cimentée par de la pyrrhotite massive ; (d) cristaux d'arsénopyrite fragmentés et cimentés par de la chalcopyrite et de la pyrrhotite massive ; (e) assemblage à bismuth natif – laïtakarite – electrum typique de la paragenèse aurifère de Salau ; (f) hédenbergite rétromorphosée en amphibole avec intercroissance de pyrrhotite disséminée dans les skarns du Bois d'Anglade ; (g) image MEB d'une apatite magmatique fragmentée contemporaine des biotites de la granodiorite de la Fourque ; (h) image MEB d'une apatite hydrothermale automorphe contemporaine de la pyrrhotite massive.*

analyzer (EA) at the LEHNA laboratory according to the protocol developed by Fourel *et al.* (2014). The mass spectrometer was of the IsoPime100 type and the elemental analyzer of the Pyrocube type in NCS combustion mode, marketed by the company Elementar. The particularity of the elemental analyzer used is to implement the technique of separating the gases to be analyzed, of the "purge and trap" type, particularly suitable for measuring the isotope ratios of sulfur (Fourel et al., 2014). Each sample was analyzed two to three times for quality control. For the calibration, 3 silver sulphide reference materials provided by the IAEA: IAEA-S1 (δ^{34}S CDT = −0.3‰), IAEA-S2 (δ^{34}S CDT = +22.7‰) and IAEA-S3 (δ^{34}S CDT = −32.3‰) were used to frame the values of the unknown samples. The values of the isotope ratios are expressed in δ^{34}S relative to the CDT standard (Tab. 1). Sulfur concentrations were calculated from elemental analyzer TCD data.

δ^{34}S ratios obtained define a wide range of values, from −0.42‰ to 18.14‰. Pyrites of the metasedimentary host rocks (Fig. 2) have the widest range with low values for the Silurian schists (−0.42‰) or the Salau marbles (4.86‰), and high values for the Mont Rouch schists (18.14‰). These results are consistent with the domain of sedimentary sulphides (Fig. 8). In the same figure, Saube (4.18‰) and Hoque Rabe (6.36‰) sphalerites fit with the volcanic sulfur source field, which is in agreement with their origin interpreted as volcano-sedimentary (Bois and Pouit, 1976; Pouit, 1984; Cugerone *et al.*, 2018). In the Salau deposit, disseminated pyrrhotite of the calcic silicate skarn reach a value of 5.01‰. Massive sulphides from the Veronique fault show spread but close values: 4.56 to 5.12‰ (arsenopyrite), 1.22 to 4.85‰ (pyrrhotite) and 2.83 to 5.22‰ (chalcopyrite). These very similar values show that the sulfur from the sulphides of the two ore types is likely of magmatic origin, a conclusion that can be extended to the massive sulphides of Aurenère (arsenopyrite 1.36‰ and pyrrhotite 1.26‰). Finally, the massive pyrrhotite from Bassiès and the pyrrhotite from Plabidaous show higher values (7.63‰ and 7.29‰) but which still correspond to the domain of magmatic sulfur, with probably a participation of a sedimentary or metamorphic sulfur source (Rye and Ohmoto, 1974).

8 Discussion

8.1 Polyphase evolution of the Salau deposit

In the Salau region, the mineralized occurrences studied belong to two distinct types of mineralization, a skarn and a vein breccia, with different geometry, mineralogy and grades. They occur as several mineralized bodies and depend on the host rock nature and its proximity to the Veronique fault.

The skarn mineralization corresponds to the orebodies of the Bois d'Anglade sector, located in embayments of the complex geometry between the granodiorite and metasedimentary host rocks. They consist of calcic silicates (garnet, hedenbergite), rare fine-grained scheelite and disseminated sulphides (arsenopyrite, pyrrhotite). Grades are generally below 0.5% WO_3 and are close to the detection threshold for gold (0.1 g/t). The prograde stage is marked by an assemblage of grossular, diopside, hedenbergite and fine-grained scheelite (< 100 μm). The retrograde stage is then marked by an epidotization of the grossular, which is also marked by alteration of the adjacent granodiorite and by the replacement of the clinopyroxene by ferroactinote. Disseminated sulphides (pyrrhotite, arsenopyrite) also occur in the grain boundaries of calcic silicates.

The vein breccia mineralization located along the E-W 70°N trending Veronique fault, has no calcic silicates and completely differs from the skarns sensu stricto (Meinert *et al.*, 2005). This vein breccia consists mainly of massive sulphides with abundant coarse-grained scheelite in cement of host rocks clasts. Field criteria show that this mineralization is clearly posterior to the skarns, and cross cut both granodiorite, marble host rocks and skarns, also confirmed by U-Pb geochronology (Poitrenaud *et al.*, 2019). Tungsten and gold contents of this vein breccia are high (> 1.5% WO_3 and 5–10 g/t Au) and correlated with massive sulphides. From a mineralogical point of view, the assemblage consists of coarse-grained scheelite (> 200 μm) and massive arsenopyrite, cross cut by a procession of dominant massive pyrrhotite, chalcopyrite, sphalerite, galena, euhedral apatite, native bismuth, electrum, bismuthinite, hessite, laitakarite, tetrahedrite and native silver.

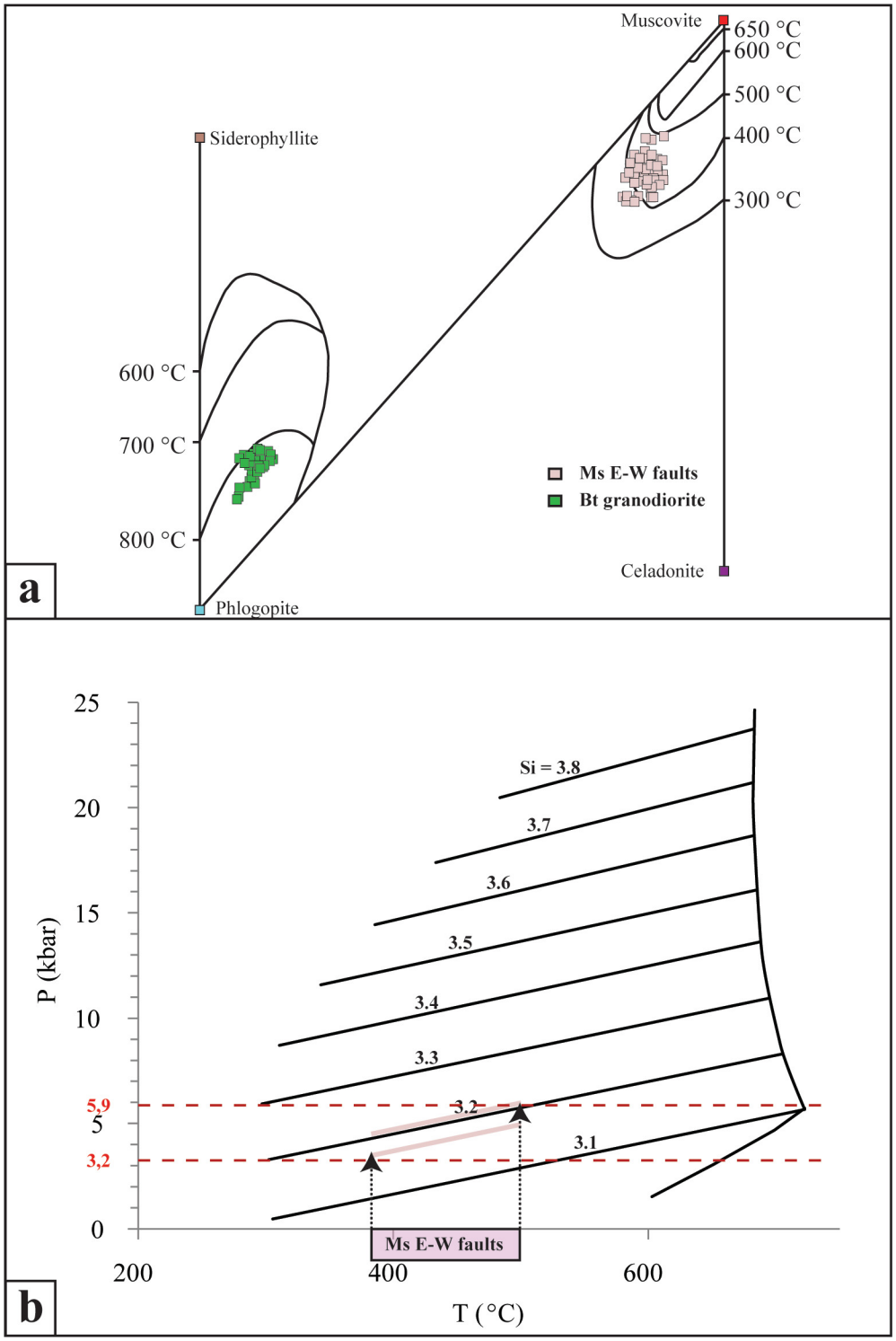

Fig. 7. (a) Monier and Robert (1986) diagram to evaluate the temperature of crystallization of black and white micas from their content in Fe and Mg; (b) Velde (1965) diagram modified by Massone and Schreyer (1987) to evaluate the H_2O pressure conditions (kbar) during white mica crystallization.

Fig. 7. *(a) Diagramme de Monier and Robert (1986) permettant de déterminer les températures des micas blancs et noirs à partir de leur richesse en Fe et en Mg ; (b) Diagramme de Velde, (1965) modifié par Massone and Schreyer, (1987) permettant de déterminer la pression H_2O (en kbar) de la cristallisation des micas blancs.*

Table 1. Table of $\delta^{34}S$ assays realized on different sulphides of the Salau deposit, adjacent mineralized occurrences and metasedimentary host rocks. The column $\delta^{34}S$ CDT is the average of the *n* analyses performed.
Tableau 1. *Table des analyses réalisées pour la mesure du $\delta^{34}S$ dans différents sulfures du gisement de Salau, des indices minéralisés voisins et de l'encaissant métasédimentaire. La colonne $\delta^{34}S$ CDT est la moyenne des* n *analyses réalisées.*

Sample number	Description	Location	$\delta^{34}S_{CDT}$	$SD_{\delta34S}$	*n*	%Save	SD%S
IAEA-S1	Standard		0.03	0.08	7	15.65	0.36
IAEA-S2	Standard		22.48	0.13	5	16.25	1.14
IAEA-S3	Standard		-32.56	0.24	5	15.53	0.19
SC1	Massive arsenopyrite	Salau	4.56	0.14	3	22.51	1.76
C1	Massive arsenopyrite	Salau	5.12	0.00	3	15.59	1.39
TP053	Massive pyrrhotite	Salau	1.22	0.10	3	33.29	0.70
TP488	Massive pyrrhotite	Salau	4.85	0.03	3	17.13	1.24
TP488	Massive chalcopyrite massive in quartz vein	Salau	5.22	0.02	3	4.06	0.32
TP432	Massive chalcopyrite	Salau	2.83	0.12	2	29.78	2.29
TP203	Disseminated pyrhotite in calcic silicates skarn	Salau	5.01	0.03	2	2.58	0.25
TP236	Pyrite vein / Pyrrhotite	Plabidaous	7.29	0.11	3	6.08	0.68
TP721A	Massive arsenopyrite	Aurenere	1.36	0.11	3	21.87	0.38
TP724	Massive pyrrhotite	Aurenere	1.26	0.16	3	24.39	0.62
BAS01	Massive pyrrhotite	Bassies	7.63	0.18	3	33.83	0.75
TP071	Sphalerite stockwerk	Hoque Rabe	6.36	0.09	3	33.26	0.64
TP170	Sphalerite stockwerk	Saube	4.18	0.16	3	35.46	0.30
TP444	Disseminated pyrite in Mont Rouch schists	Mont Rouch	18.14	0.21	3	2.27	0.25
TP109	Disseminated pyrite in Salau marbles	Marbre Salau	4.86	0.47	3	0.55	0.34
TP10	Disseminated pyrite in Silurian black schists	Couflens	-0.42	0.15	2	2.64	0.09

3D modeling of the exploitation drillholes shows that the two skarn compartments of the Veronique district (developments at levels 1450 and 1230) are sectioned by the Veronique fault with a reverse dextral movement and an offset of more than 200 m. The kinematic, deduced from the shear criteria observed at the surface or in mining works, is consistent with the offset of the mineralized bodies in the 3D model. The Veronique fault is regionally connected to multikilometric shear corridors described throughout the Axial Zone (Cochelin *et al.*, 2018). However, far from the Salau mine area, the fault does not contain any trace of mineralization. Thus, away from La Fourque pluton, as in Plagnau long ravine and in the Pallaresa valley, the extension of the Veronique fault is only represented by a barren pyritic breccia. The mineralization is therefore not only controlled by the regional faults but also by the proximity of the intrusion. The faults potentially localize fluid circulation while the heat provided by the La Fourque pluton at the time of emplacement is probably the source of hydrothermal circulation (Marcoux *et al.*, 2015).

In the Salau deposit, massive sulphides are closely related to aplite dyke swarms and tourmaline veins which cross cut the base of La Fourque granodiorite, as shown by their progressive lateral transition to massive sulphides. We interpret them as constituting the apical part of a second intrusion, more differentiated and underlying the La Fourque granodiorite. Such relationships between aplitic dykes and sulphide mineralization have been described at a regional scale, in particular at Bassiès (Gerbal and Ledru, 1985) and Cauterets (Ledru, 1986), but also in Canada (Cantung; Rasmussen, 2004; Rasmussen *et al.*, 2011) and in Russia (Lermontovskoe deposit; Soloviev *et al.*, 2017a; Vostok-2 deposit, Soloviev *et al.*, 2017b; Skrytoe deposit, Soloviev and Kryazhev, 2017c). The assemblage of native bismuth, bismuthinite and Pb-Bi and Cu-Bi sulfosalts shows a stronger affinity with late evolved magmas than with intermediate magmas (Derré *et al.*, 1980; Ciobanu *et al.*, 2010; Cepedal *et al.*, 2013; Botros, 2015).

Datings combined with the composition of fluid inclusions (Krier-Schellen, 1988; Poitrenaud *et al.*, 2019), indicate two different mineralizing episodes which take place successively under conditions of decreasing temperatures and changes in the fluid composition (Fig. 9). The results on magmatic zircon show that the emplacement of granodiorite, at the origin of the scheelite skarn, occurred at 295 ± 2 Ma (Poitrenaud *et al.*, 2019). The P-T conditions of emplacement for the granodioritic intrusion of the Fourque, obtained from microprobe analyzes on black mica and amphibole in this study show a temperature above 800 °C for a pressure of 2.5 to 3 kbar (8 to 10 km depth). These results for the granodiorite intrusion are consistent with the estimations for skarn formation temperature obtained by thermodynamics (505–540 °C; Soler, 1977), fluid inclusions (microthermometric data: 470–530 °C; Krier-Schellen, 1988) and RSCM (600–650 °C; Poitrenaud, 2018). This first generation of fluid, linked to the formation of skarns, essentially consists of a highly saline H_2O–NaCl solution (25 wt.% Eq. NaCl), with halite crystals, typical of a magmatic origin (Krier-Schellen, 1988). The high temperatures and the geological context confirmed that it is a magmatic fluid.

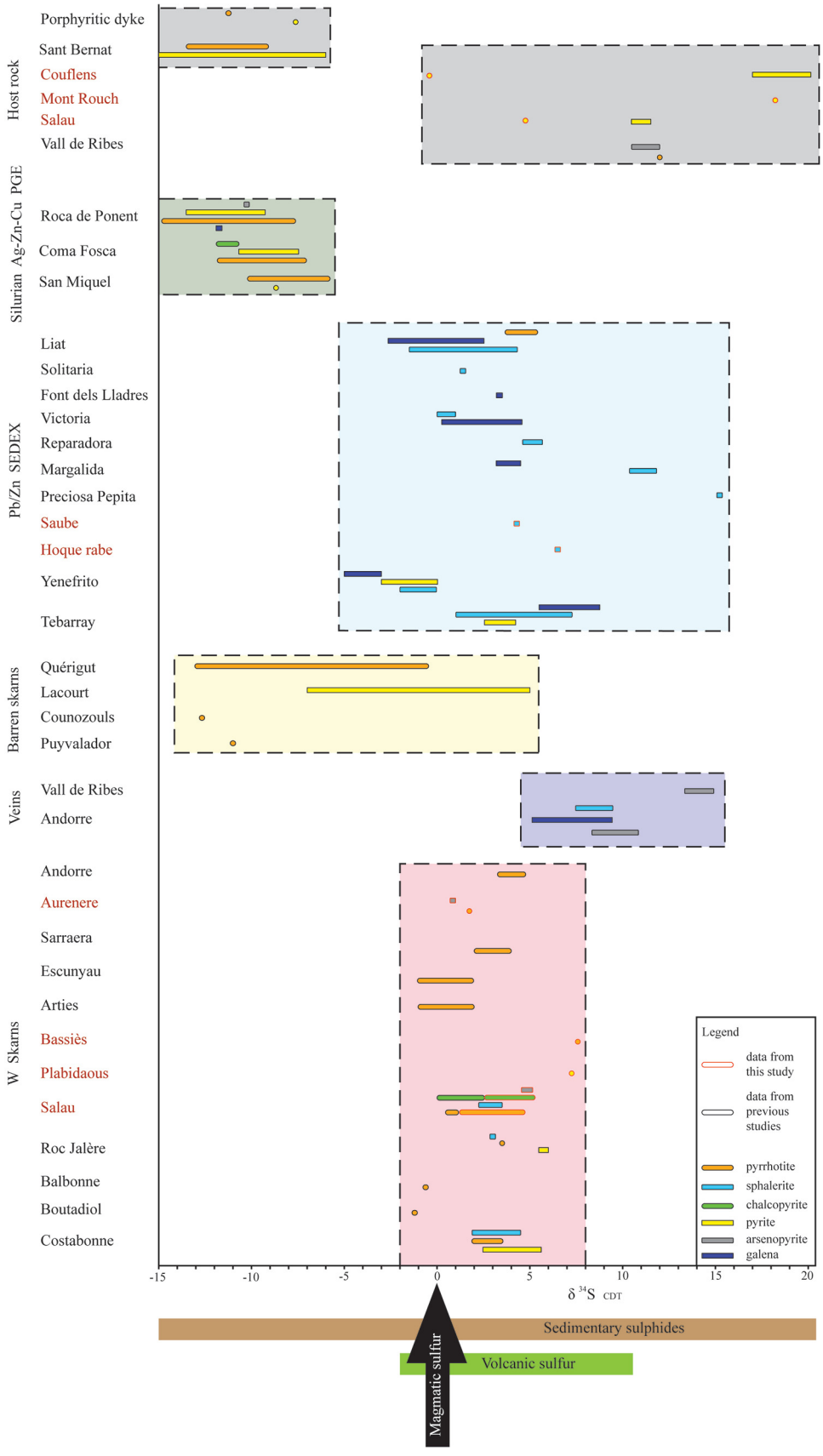
Host rock
Porphyritic dyke
Sant Bernat
Couflens
Mont Rouch
Salau
Vall de Ribes
Silurian Ag-Zn-Cu PGE
Roca de Ponent
Coma Fosca
San Miquel
Pb/Zn SEDEX
Liat
Solitaria
Font dels Lladres
Victoria
Reparadora
Margalida
Preciosa Pepita
Saube
Hoque rabe
Yenefrito
Tebarray
Barren skarns
Quérigut
Lacourt
Counozouls
Puyvalador
Veins
Vall de Ribes
Andorre
W Skarns
Andorre
Aurenere
Sarraera
Escunyau
Arties
Bassiès
Plabidaous
Salau
Roc Jalère
Balbonne
Boutadiol
Costabonne
Legend
data from this study
data from previous studies
pyrrhotite
sphalerite
chalcopyrite
pyrite
arsenopyrite
galena
-15
-10
-5
0
5
10
15
20
δ 34S CDT
Sedimentary sulphides
Volcanic sulfur
Magmatic sulfur

Fig. 8. Compilation of $\delta^{34}S$ CDT assays realized for this study and for sulphides from different mineralizations through the axial zone of the Pyrenees (data compiled from Guy, 1979; Soler, 1990; Soler *et al.*, 1990; Cardellach *et al.*, 1992). The orange place names correspond to the sites from which the samples analyzed in this study were collected, while the black place names correspond to the sites from which the data was extracted in the existing literature. The result of the analyzes performed in this study is represented by a red box in the figure. The $\delta^{34}S_{CDT}$ compositional domains of magmatic, volcanic and sedimentary sulfur were compiled from Lancelot *et al.* (1971), Rye and Ohmoto (1974) and Seal (2006).

Fig. 8. *Compilation de mesures de $\delta^{34}S_{CDT}$ réalisées dans cette étude et pour les sulfures de différentes minéralisations à travers la zone axiale des Pyrénées (données compilées d'après Guy, 1979 ; Soler, 1990 ; Soler* et al.*, 1990 ; Cardellach* et al.*, 1992). Les noms de lieu en orange correspondent aux sites d'où proviennent les échantillons analysés dans cette étude alors que les noms de lieu en noir correspondent à des sites d'où ont été extraites les données de la littérature existante. Le résultat des analyses réalisées dans cette étude est représenté par un encadré rouge sur la figure. Les domaines de composition du $\delta^{34}S_{CDT}$ du soufre magmatique, volcanique et sédimentaires sont compilés de Lancelot* et al. *(1971), Rye and Ohmoto (1974) et Seal (2006).*

Datings of hydrothermal apatite grains from massive sulphides ore show an age of 289.1 ± 1.9 Ma, younger than the formation of the skarn (Poitrenaud *et al.*, 2019). Therefore, the two types of ore are separated by a minimum of about 2 Ma and a maximum of about 9 Ma. The second generation of fluid inclusions observed in the coarse-grained scheelites and quartz associated with the massive sulphides hosted by the Veronique fault show two types of solutions, one with H_2O–NaCl identical to the fluid found in the skarns and the other with H_2O–CO_2–CH_4 interpreted of metamorphic origin by Krier-Schellen (1988) and Fonteilles *et al.* (1989). The temperatures estimated by different methods are relatively consistent: thermochemistry (450 °C, Soler, 1977; 327–366 °C, Zahm, 1987), fluid inclusions (335–363 °C for 2.4 kbar, Krier-Schellen, 1988) or microchemistry on phengites in shear zones for this study (400 °C to 500 °C for a pressure of 3.2 to 5.9 kbar). The pressure interval obtained on phengites is intrinsically explained by the degree of precision provided with the thermometric diagram of Monier and Robert (1986). Phengites were collected from the same type of shear zones and show temperatures of 400 °C to 500 °C. The impact of this temperature interval is important in the diagram of Massone and Schreyer (1987) due to the high-pressure variation for a small temperature variation, which explains the wide pressure range obtained (3.2 to 5.9 kbar).

In mineralized systems, a method to identify the source of the fluids is to evaluate the isotopic fractionation of stable elements which enter into their composition, such as sulfur, carbon or oxygen (Rye and Ohmoto, 1974; Höll *et al.*, 1987; Ishihara and Sasaki, 1989; Coplen and Krouse, 1998; Seal, 2006; Yang and Lentz, 2010; Sharman *et al.*, 2014; Tanner *et al.*, 2016). The sulfur isotopic values obtained in this study have been compared with a compilation of all others bibliographical results obtained on the sulphides of the axial zone of the Pyrenees (Fig. 8). This comparison show that the sulphides from the metasedimentary host rocks (Vall de Ribes, Salau and San Bernat) have a $\delta^{34}S$ spread over a wide range of values (−15 to +20‰), which fit the composition domain of sedimentary sulfur. Ag–Zn–Cu mineralizations of the Silurian black shales (Roca de Ponent, Coma Fosca, San Miquel (Pura *et al.*, 2002) also show $\delta^{34}S$ values, typical of sulfur from sedimentary origin (−15‰ to −5‰), while most lead-zinc SEDEX in the axial zone (deposits of Liat, Solitaria, Font dels Lladres, Victoria, Reparadora, Preciosa Pepita, Saube, Hoque Rabe, Yenefrito, Tebarray), with a few exceptions (Margalida deposit +10 to +12‰, Preciosa Pepita deposit +16‰; Cardellach *et al.*, 1996), show values between −3‰ and +10‰ in agreement with sulfur from volcanic origin. Pyrrhotite and pyrite of the barren skarns developed around the intrusions of Quérigut, Lacourt, Counozouls and Puyvalador (Guy, 1979; Toulhoat, 1982) have very low values (−13‰ to +2‰). The origin of the latter can result from a mix between magmatic and sedimentary sulfur. Auriferous veins with quartz-arsenopyrite from Andorra and Vall de Ribes show values between +5‰ and +15‰. Their signature shows a possible metamorphic influence. Some authors described them as retrograde shear zones (Ayora *et al.*, 1992; Ayora and Casas, 1995). Finally, the sulphides of mineralized skarns and massive sulphide breccias from the deposits and occurrences of Andorra, Aurenere, Sarraera, Escunyau, Arties, Bassiès, Salau, Roc Jalère, Balbonne, Boutadiol and Costabonne (Guy, 1979; Soler, 1990; Soler *et al.*, 1990; Cardellach *et al.*, 1992) show relatively low values, between −2‰ and +8‰, which contribute to consider a sulfur from magmatic origin.

8.2 Metallogenic model

All these results converge to propose a two-stage model for the formation of the Salau deposit (Figs. 9 and 10). This model is consistent with the regional geological context of the Axial Zone and fits perfectly into the polyphase evolution described by Denèle *et al.* (2014) and Cochelin *et al.* (2018). The intrusion of La Fourque granodiorite is synchronous (295 ± 2 Ma) with most of the calc-alkaline plutons emplaced between 305–295 Ma during an N-S isoclinal folding episode of the Axial Zone. The emplacement P-T conditions are 800 °C and 3.3 kbar. Calcic silicate skarns, with rare fine-grained scheelite and disseminated sulphide, were developed on its border at contact with the Devonian marble host rocks, during cooling. The tungsten contents are low (< 0.5% WO_3) and gold is absent. During the general cooling of the Variscan crust, the regional deformation is localized at the level of rheological contrasts (granitoid contact – surrounding and at periphery of metamorphic domes) along dextral reverse shear zones. These shear zones appear later, at 289 ± 2 Ma in Salau and Aurenère. A second mineralization (massive sulphides, abundant coarse-grained scheelite and gold) with high tungsten and gold contents (> 1.5% WO_3 and 10 g/t Au) is hosted by these faults and deposited at about 450 °C and 3.2 to 5.9 kbar. Associated fluids come from a swarm of aplite dykes which constitute the apical part of a second intrusion, leucogranitic and more differentiated.

The Salau deposit therefore reflects the Carboniferous-Lower Permian evolution of the Variscan crust in the Axial

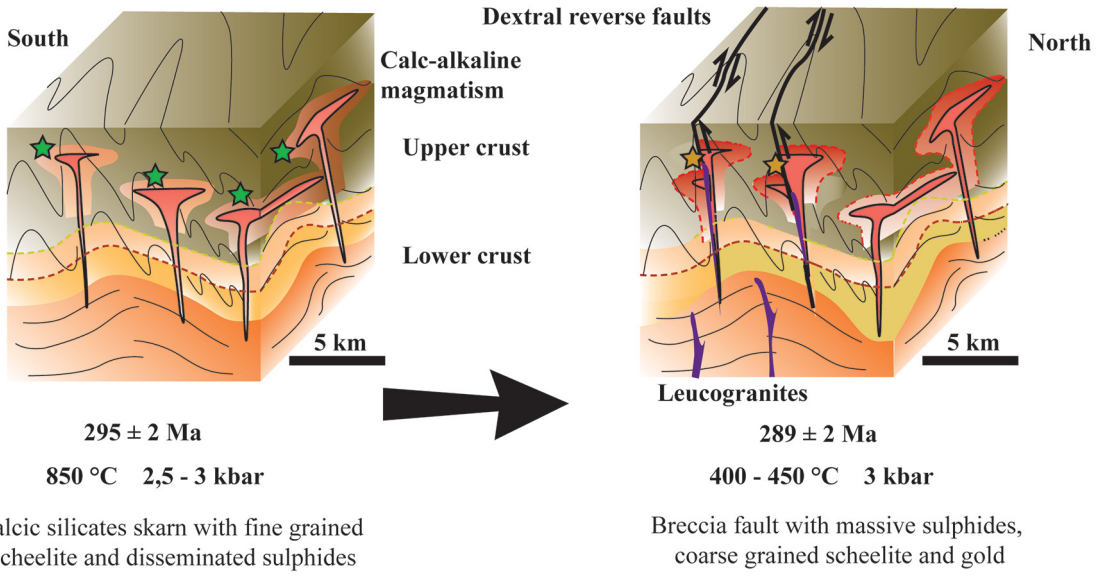

Fig. 9. Chronological diagram of the genesis of the Salau ore deposit at the scale of the upper and medium crust of the axial zone of the Pyrenees. A N-S compression stage led to the formation of N110°E folds, the intrusion of the Fourque granodiorite and the genesis of the associated scheelite skarn ca. 295 Ma. A second stage, ca. 289 Ma corresponds to the intrusion of a late evolved granite and to the appearance of the deformation in shear zones during the gradual cooling of the crust leading to the formation of coarse scheelite, massive sulphides and gold mineralization in the brecciated veins.

Fig. 9. *Schéma chronologique de la genèse du gisement de Salau à l'échelle de la croûte supérieure et moyenne dans la zone axiale des Pyrénées. Un stade de compression N-S conduit à la formation de plis N110°E, à l'intrusion de granodiorite de la Fourque et à la genèse du skarn à scheelite associé vers 295 Ma. Un deuxième stade, vers 289 Ma, correspond à l'intrusion d'un granite évolué tardif et à l'apparition de la déformation dans des zones de cisaillement durant le refroidissement progressif de la croûte conduisant à la formation de scheelite grossière, de sulfures massifs et de la minéralisation aurifère dans les brèches filoniennes.*

Zone and show the transition from a homogeneous thickening stage of the upper crust, while the lower crust is partially molten, towards a system where the deformation is localized at the level of EW reverse dextral faults which drain W-Au fluids of more evolved magmas. At the scale of the Axial Zone of the Pyrenees, many calc-alkaline intrusive massifs are cross cut by swarms of dykes or even small stocks of leucogranites (Gleizes, 1992; Barnolas and Chiron, 1996; Gleizes *et al.*, 1997; Roberts *et al.*, 2000; Aleksandrov and Troneva, 2011; Olivier *et al.*, 2016). Similar occurrences to the Salau deposit with the spatial and temporal superposition of two mineralization types have also been described for the intrusions of Bassiès (Poitrenaud, 2018) or Aurenère (Spain; Palau i Ramirez *et al.*, 1997; Poitrenaud *et al.*, 2019).

The Salau deposit has many similarities with the Mactung and Cantung deposits in Canada (Dick and Hodgson, 1982; Rasmussen, 2004; Rasmussen *et al.*, 2011). The geological context is very similar between these Canadian deposits and Salau with polyphase intrusions, granodioritic and then leucogranitic in a carbonate metasedimentary series. Their sulphide sequence with pyrrhotite, chalcopyrite, arsenopyrite and sphalerite, posterior to the skarns, are identical to Salau with in particular native bismuth associated with gold (Palmer *et al.*, 2013; Lentz *et al.*, 2015). Their genesis is similar with an early metasomatic stage which develops skarns with a low tungsten content (0.2 to 0.5% WO_3) followed by a late hydrothermal stage, associated to a sulphide mineralization rich in scheelite (> 1% WO_3; Hodgson, 2000), linked to faults and to a more differentiated late granitic intrusion. Only the age and the geodynamic context of the intrusion differ: late Variscan for Salau and Cretaceous for the Yukon skarns.

The massive sulphide, coarse-grained scheelite and gold mineralization hosted by the Veronique fault, share numerous similarities with the Intrusion Related Gold Deposit model (IRGD; Hart, 2007). This recently proposed model groups a large diversity of mineralization morphology: quartz veins, sheeted or in stockwork in the Tighza deposit (Morocco; Marcoux *et al.*, 2015), veins or disseminated in granite (Timbarra deposit, Autralia; Mustard, 2001), breccia (Kidston deposit, Australia; Baker and Andrew, 1991), greisen (Salave deposit, Spain; Harris, 1980) or skarn in contact with granite (Dublin Gulch deposit, Alaska; Maloof *et al.*, 2001). The ore morphology of the Veronique fault (massive sulphide breccia) is compatible with the type of fault described in the Ryan Lode deposit (Bakke *et al.*, 2000). The common characteristic of all these mineralizations is their magmatic origin, frequently marked by a mineral assemblage which contains metals and lithophilic elements such as arsenic, tungsten, tin, molybdenum, bismuth, tellurium, gold, silver and antimony (Thompson *et al.*, 1999; Thompson and Newberry, 2000; Lang and Baker, 2001; Hart, 2007). The massive sulphide ore also shows very good correlations between tungsten, bismuth, tellurium and gold contents. The second generation of fluid inclusions observed in coarse-grained scheelites and quartz in massive sulphides ore from the Veronique fault is a solution with H_2O–CO_2–CH_4 (Krier-Schellen, 1988; Fonteilles *et al.*, 1989), characteristic of fluids rich in CH_4, resulting from reduced plutons of the ilmenite series (Zhang *et al.*, 2019). Finally,

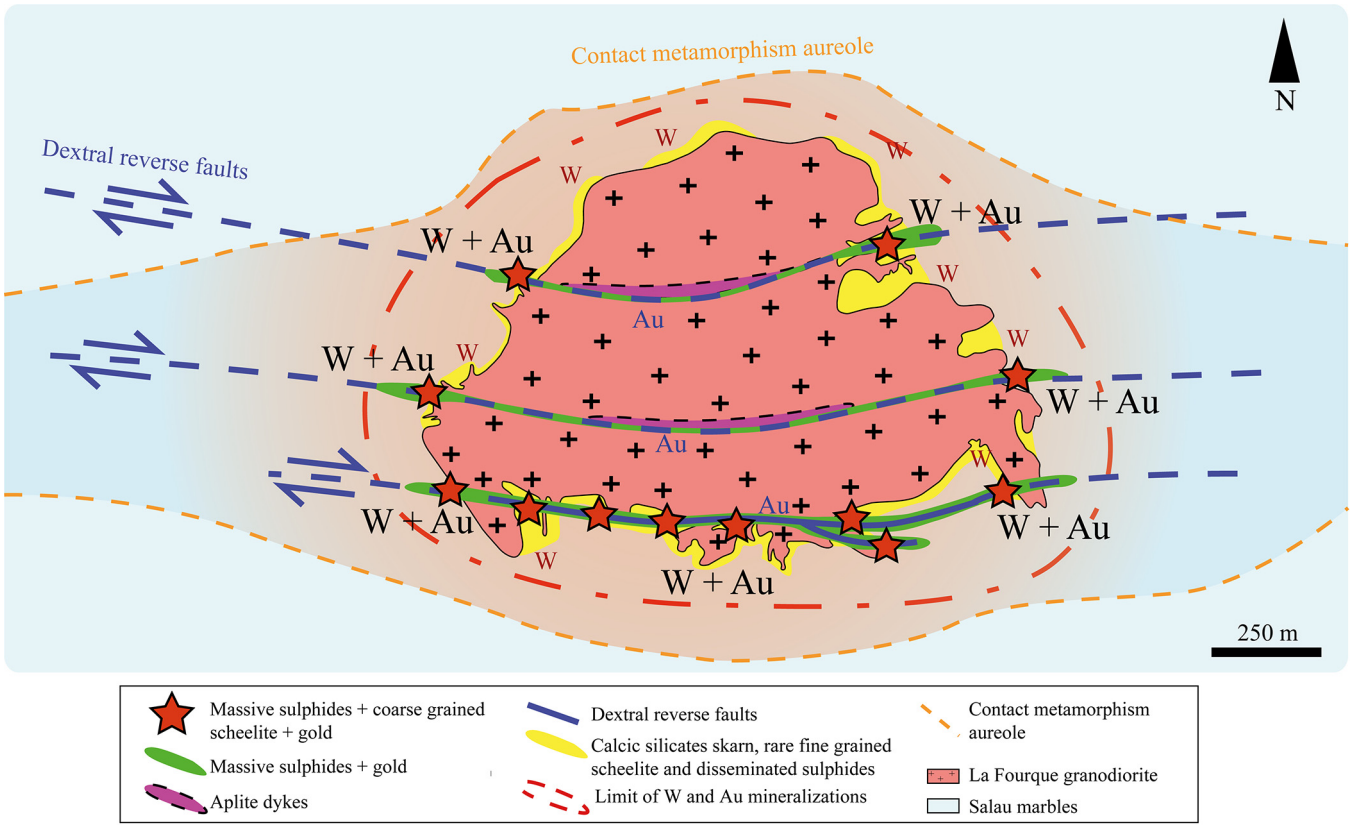

Fig. 10. Summary map of the different mineralizations observed at the Salau ore deposit.
Fig. 10. *Carte de synthèse des différentes minéralisations observées au niveau du gisement de Salau.*

mineralization is not only controlled by regional faults but essentially by the distance to the intrusion. All these criteria converge to classify the Salau deposit in the Intrusion Related Gold Deposit (IRGD) model.

9 Conclusions

Main results of our work show that:

1 two different types of mineralization coexist at Salau (Fig. 10), a skarn with calcic silicates, fine-grained scheelite and disseminated sulphides (arsenopyrite, pyrrhotite) developed around La Fourque intrusion emplaced at 800 °C and 3.3 kbar at 295 ± 2 Ma, as well as a vein breccia with massive sulphide, coarse-grained scheelite and gold hosted by the Veronique fault, emplaced at 450 °C and 3.2 to 5.9 kbar at 289 ± 2 Ma. These two mineralizations have mineralogical characteristics, peri-intrusion locations, morphology and emplacement in decreasing temperature conditions which link them to an IRGD model;
2 the coexistence of two types of mineralization also results from a magmatic polyphase, like the copper porphyry systems, the source of the vein breccia mineralization with high tungsten and gold content being linked to the emplacement of an evolved leucogranite which ascent in the upper crust through regional EW faults;
3 the evolution of mineralizing phenomenon in the Salau deposit reflects the dynamics of the differentiation at depth of late Variscan magmatism in the axial zone of the Pyrenees.

The polyphase evolution of the Salau deposit is fully in line with the late Variscan evolution of the Paleozoic basement of the Pyrenees and reflects the differentiation dynamics of late-orogenic Variscan, granodioritic and then leucogranitic magmatism. The granodioritic intrusion of Salau emplaced within an antiform at 3.3 kbar and 800 °C during a general shortening stage due to the closure of the Ibero-Armorican arc at ca. 295 Ma (Cochelin *et al.*, 2018). This period corresponds to the end of the metamorphic domes exhumation and is characterized by a general state of abnormally warm crust. Skarns were developed at the contact of the granodiorite during its progressive cooling. The temperature of the Paleozoic basement then gradually decrease and the deformation regime changes. The deformations previously homogeneously distributed, are then focalized within regional E-W dextral reverse shear zones developed in rheological contrasts. The periphery of metamorphic domes and calc-alkaline granitoids are particularly suitable. In these shear zones, differentiated intrusions, like leucogranites, rise in the upper crust at ca. 289 Ma as the last residual melt extracted from a deep magma chamber. A massive sulphide, coarse-grained scheelite and gold mineralization was developed in the faults which act as a drain and cross cut the earlier skarns with a plurikilometric offset under P-T conditions of 450 °C and 3.2 to 5.9 kbar. The Salau deposit is a skarn over which a massive sulphide breccia, rich in tungsten and gold, is superimposed. According to numerous geochemical, genetic and structural criteria, it reflects the evolution of an Intrusion Related Gold Deposit (IRGD) model.

Supplementary Material

Fig. 1. Optical microscopy images using polarized and analyzed light of white micas studied with the microprobe: (a) TP627 - (b) TP492 - (d) TP752a: neocrystallized phengites from plagioclases during the shearing of the granodiorite by the Véronique fault; (c) TP492: Neoformed sigmoidal phengites in granodiorite and sheared with quartz recrystallization in pressure shadow.
Tab. 1. Analytical results table and corresponding calculated pressures of the biotites from the La Fourque granodiorite with the equation of Uchida *et al.* (2007) (data compiled from Lecouffe, 1987).
Tab. 2. Result of microprobe analyzes of white mica from E-W trending shear zones (Veronique and satellite faults) intersecting the La Fourque granodiorite. N correspond to the number of analyzes.
Tab. 3. Table of analytical results by electron microprobe of the hornblendes from la Fourque granodiorite (Soler, 1977) and the corresponding pressures calculated from the equations of Hammarstrom and Zen (1986); Hollister *et al.* (1987); Johnson and Rutherford (1989); Thomas and Ernst (1990); Schmidt (1992) and Mutch *et al.* (2016).

The Supplementary Material is available at http://www.bsgf.fr/10.1051/bsgf/2020044.

Acknowledgements. Main results of this study were funded by the company e-Mines through its R&D activity and the ISTO laboratory at the University of Orleans. The authors particularly thank F. Carbalido, F. Cheval-Garabedian, Q. Monge, J.L. Carbalido, and M. Bonnemaison for their support in the field, C. Derré, P. d'Arco, A.S. Audion, M. Picault, J. Gouin, G. Raoult, and B. Cochelin for their technical support, the supply of some key samples and their expert advice, and also I. Di Carlo (ISTO) for his help with the microprobe analyzes, S. Janiec, G. Badin, and P. Benoist from the ISTO laboratory for the preparation and good quality of thin sections, polished sections and mineral separations, F. Fourel from the LEHNA laboratory of the Claude Bernard University in Lyon for sulfur isotopic analyses. L. Jolivet, O. Vanderhaeghe and the two anonymous reviewers are also thanked for their constructive remarks to improve this manuscript.

References

Aguilar C, Liesa M, Castineiras P, Navidad M. 2013. Late Variscan metamorphic and magmatic evolution in the eastern Pyrenees revealed by U–Pb age zircon dating. *Journal of the Geological Society, London* 171: 181–192.

Aleksandrov SM, Troneva MA. 2011. Genesis and Composition of Endogenous Borates in the Skarns of the Eastern and Central Pyrenees. *Geochemistry International* 49(8): 802–814. https://doi.org/10.1134/S0016702911080027.

Auréjac JB, Gleizes G, Diot H, Bouchez JL. 2004. Le complexe granitique de Quérigut (Pyrénées, France) ré-examiné par la technique de l'ASM : un pluton syntectonique de la transpression dextre hercynienne. *Bulletin de la Société Géologique de France* 175: 660–661.

Autran A, Fonteilles M, Guitard G. 1970. Relations entre les intrusions de granitoïdes, l'anatexie et le métamorphisme régional, considérées principalement du point de vue du rôle de l'eau : cas de la chaine hercynienne des Pyrénées orientales. *Bulletin de la Société Géologique de France* 7(XII): 673–731.

Ayora C, Ribera F, Cardellach E. 1992. The genesis of the arsenopyrite gold veins from the Vall de Ribes District, eastern Pyrenees, Spain. *Economic Geology and the Bulletin of the Society of Economic Geologists* 87(7): 1877–1896. https://doi.org/10.2113/gsecongeo.87.7.1877.

Ayora C, Casas JM. 1995. Strata-bound As-Au mineralization in pre-Caradocian rocks from the Vall de Ribes, eastern Pyrenees, Spain. *Mineralium Deposita* 21(4): 278–287.

Baker EM, Andrew AS. 1991. Geologic, fluid inclusion, and stable isotope studies of the gold-bearing breccia pipe at Kidston, Queensland, Australia. *Economic Geology and the Bulletin of the Society of Economic Geologists* 86(4), 810–830. https://doi.org/10.2113/gsecongeo.86.4.810.

Bakke A, Morrel B, Odden J, Bergstron T, Woodman J. 2000. Kinross Gold USA's activities in the Fairbanks mining district, K2K. *British Columbia and Yukon Chamber of Mines, Special Volume* 2: 89–98.

Ballouard C, Poujol M, Mercadier J, Deloule E, Boulvais P, Baele JM, *et al.* 2017. Uranium metallogenesis in the peraluminous leucogranites from the Pontivy-Rostrenen magmatic complex (French Armorican Hercynian Belt): the result of long term oxidizing hydrothermal alteration during strikeslip deformation. *Mineralium Deposita* 53: 601–628. https://doi.org/10.1007/s00126-017-0761-5.

Barnolas A, Chiron JC. 1996. Synthèse géologique et géophysique des Pyrénées – Volume 1 Introduction. Géophysique. Cycle hercynien, vol. 2. Editions BRGM-ITGE.

Bodin J, Ledru P. 1986. Nappes hercyniennes précoces à matériel dévonien hétéropique dans les Pyrénées ariégeoises. *Comptes Rendus de l'Académie des Sciences* 302(II): 969–974.

Bois JP, Pouit G. 1976. Les minéralisations de Zn (Pb) de l'anticlinorium de Pierrefitte : Un exemple de gisements hydrothermaux et sédimentaires associés au volcanisme dans le Paléozoïque des Pyrénées centrales. *Bureau Rech. Geol. Min.* 6: 543–567.

Botros NS. 2015. The role of the granite emplacement and structural setting on the genesis of gold mineralization in Egypt. *Ore Geology Reviews* 70: 173–187. https://doi.org/10.1016/j.oregeorev.2015.04.014.

Bouchez JL, Gleizes G. 1995. Two-stage deformation of the Mont-Louis-Andorra granite pluton (Variscan Pyrenees) inferred from magnetic susceptibility anisotropy. *Journal of the Geological Society, London* 152(4): 669–679. https://doi.org/10.1144/gsjgs.152.4.0669.

Boulvais P, Ruffet G, Cornichet J, Mermet M. 2007. Cretaceous albitization and dequartzification of Hercynian peraluminous granite in the Salvezines Massif (French Pyrenees). *Lithos* 93 (1-2): 89–106. https://doi.org/10.1016/j.lithos.2006.05.001.

Boutin A, de Saint Blanquat M, Poujol M, Boulvais P, de Parseval P, Rouleau C, *et al.* 2016. Succession of Permian and Mesozoic metasomatic events in the eastern Pyrenees with emphasis on the Trimouns talc-chlorite deposit. *International Journal of Earth Sciences* 105(3): 747–770. https://doi.org/10.1007/s00531-015-1223-x.

Cardellach E, Ayora C, Soler A, Delgado J, Stumpfl EF. 1992. The origin of fluids involved in the formation of gold-bearing skarns of the Andorra Granite (central Pyrenees, Spain); sulphur isotope data. *Mineralogy and Petrology* 45(3-4): 181–193.

Cardellach E, Canals A, Pujals I. 1996. La composicion isotopica del azufre y del plomo en las mineralizaciones de Zn-Pb del valle de Aran (Pirineo Central) y su significado metalogenetico. *Estudios Geológicos* 52: 189–195.

Carreras J, Capellà I. 1994. Tectonics levels in the Palaeozoic basement of the Pyrenees: a review and a new interpretation. *Journal of Structural Geology* 16(11): 1509–1524.

Cassata WS, Renne PR, Shuster DL. 2009. Argon diffusion in plagioclase and implications for thermochronometry: A case study from the Bushveld Complex, South Africa. *Geochimica et Cosmochimica Acta* 73(21): 6600–6612.

Cepedal A, Fuertes-Fuente M, Martin-Izard A, Garcia-Nieto J, Boiron M-C. 2013. An intrusion-related gold deposit (IRGD) in the NW of Spain, the Linares deposit: Igneous rocks, veins and related alterations, ore features and fluids involved. *Journal of Geochemical Exploration* 124: 101–126.

Charles N, Augier R, Gumiaux C, Monié P, Chen Y, Faure M, *et al.* 2013. Timing, duration and role of magmatism in wide rift systems: Insights from the Jiaodong Peninsula (China, East Asia). *Gondwana Research* 24(1): 412–428.

Ciobanu CL, Birch WD, Cook NJ, Pring A, Grundler PV. 2010. Petrogenetic significance of Au-Bi-Te-S associations: The example of Maldon, Central Victorian gold province, Australia. *Lithos* 116: 1–17. https://doi.org/10.1016/j.lithos.2009.12.004.

Cochelin B. 2016. Champ de déformation du socle paléozoïque des Pyrénées. Thèse de l'Université Toulouse 3 Paul Sabatier.

Cochelin B, Lemirre B, Denèle Y, de Saint Blanquat M, Lahfid A, Duchêne S. 2018. Structural inheritance in the Central Pyrenees: the Variscan to Alpine tectonometamorphic evolution of the Axial Zone. *Journal of the Geological Society, London* 175: 336–351. https://doi.org/10.1144/jgs2017-066.

Colchen M, Ternet Y, Debroas EJ, Dommanget A, Gleizes G, Guérangé B, *et al.* 1997. Carte géologique de la France (1/50 000), feuille Aulus-les-Bains (1086). Orléans: Editions BRGM.

Coplen TB, Krouse HR. 1998. Sulphur isotope data consistency improved. *Nature* 392: 32.

Cowan EJ. 2020. Deposit-scale structural architecture of the Sigma-Lamaque gold deposit, Canada – Insights from a newly proposed 3D method for assessing structural controls from drill hole data. *Mineralium Deposita* 55: 217–240.

Cugerone A, Oliot E, Chauvet A, Gavaldà Bordes J, Laurent A, Le Goff E, *et al.* 2018. Structural control on the formation of Pb-Zn deposits: An example from the Pyrenean Axial Zone. *Minerals* 8 (489): 20. https://doi.org/10.3390/min8110489.

Cugerone A, Cenki-Tok B, Oliot E, Munoz M, Barou F, Motto-Ros V, *et al.* 2020. Redistribution of germanium during dynamic recrystallization of sphalerite. *Geology* 48(3): 236–241.

Debon F, Guitard G. 1996. Carte de synthèse, métamorphisme et plutonisme hercyniens. In: *Synthèse géologique et géophysique des Pyrénées*, vol. 1. Éditions BRGM-ITGE.

Delchini S, Lahfid A, Plunder A, Michard A. 2016. Applicability of the RSCM geothermometry approach in a complex tectono-metamorphic context: The Jebilet massif case study (Variscan Belt, Morocco). *Lithos* 256-257: 1–12. https://doi.org/10.1016/j.lithos.2016.04.007.

Deloule E, Alexandrov P, Cheilletz A, Laumonier B, Barbey P. 2002. In-situ U-Pb zircon ages for Early Ordovician magmatism in the eastern Pyrenees, France; the Canigou Orthogneisses. *International Journal of Earth Sciences* 91(3): 398–405. https://doi.org/10.1007/s00531-001-0232-0.

Denèle Y, Olivier P, Gleizes G, Barbey P. 2007. The Hospitalet gneiss dome (Pyrenees) revisited: lateral flow during Variscan transpression in the middle crust. *Terra Nova* 19(6): 445–453. https://doi.org/10.1111/j.1365-3121.2007.00770.x.

Denèle Y, Olivier P, Gleizes G. 2008. Progressive deformation of a zone of magma transfer in a transpressional regime: The Variscan Mérens shear zone (Pyrenees, France). *Journal of Structural Geology* 30(9): 1138–1149. https://doi.org/10.1016/j.jsg.2008.05.006.

Denèle Y, Olivier P, Gleizes G, Barbey P. 2009a. Decoupling between the middle and upper crust during transpression-related lateral flow: Variscan evolution of the Aston gneiss dome (Pyrenees, France). *Tectonophysics* 477(3-4): 244–261. https://doi.org/10.1016/j.tecto.2009.04.033.

Denèle Y, Barbey P, Deloule E, Pelleter E, Olivier P, Gleizes G. 2009b. Middle Ordovician U-Pb age of the Aston and Hospitalet orthogneissic laccoliths: their role in the Variscan evolution of the Pyrenees. *Bulletin de la Société Géologique de France* 180(3): 209–216. https://doi.org/10.2113/gssgfbull.180.3.209.

Denèle Y, Paquette JL, Olivier P, Barbey P. 2011. Permian granites in the Pyrenees: The Aya pluton (Basque Country). *Terra Nova* 24(2): 105–113. https://doi.org/10.1111/j.13653121.2011.01043.x.

Denèle Y, Laumonier B, Paquette JL, Olivier P, Gleizes G, Barbey P. 2014. Timing of granite emplacement, crustal flow and gneiss dome formation in the Variscan segment of the Pyrenees. *Geological Society of London* 405: 265–287. https://doi.org/10.1144/SP405.5.

Derré C. 1973. Relations chronologiques entre la mise en place du granite de Salau (Haute Vallée du Salat, Pyrénées ariégeoises) et les déformations du Paléozoïque de la région. *Comptes Rendus de l'Académie des Sciences* 277(D): 1279–1281.

Derré C, Fonteilles M, Nansot YL. 1980. Le gisement de scheelite de Salau, (Ariège, Pyrénées). In: *26e CGI Gisements français*, Paris, Fasc. E9, 42 p.

Derré C. 1982. Caractéristiques de la distribution des gisements à étain et tungstène dans l'Ouest de l'Europe. *Mineralium Deposita* 17: 55–77.

Derré C, Lafitte M, Maury R. 1984. Etude des minéralisations sulfurées du gisement de Salau, Pyrénées (France) et de ses environs. *Mineralium Deposita* 19: 176–182.

Dick LA, Hodgson CJ. 1982. The MacTung W-Cu (Zn) contact metasomatic and related deposits of the northeastern Canadian Cordillera. *Economic Geology* 77: 845–867.

Einaudi MT, Meinert LD, Newberry RJ. 1981. Skarn deposits. *Economic Geology 75th Anniversary Volume:* 317–391.

Einaudi MT, Burt DM. 1982. Introduction-terminology, classification, and composition of skarn deposits. *Economic Geology* 77: 745–754.

Evans NG, Gleizes G, Leblanc D, Bouchez JL. 1997. Hercynian tectonics in the Pyrenees: a new view based on structural observations around the Bassiès granite pluton. *Journal of Structural Geology* 19(2): 195–208. https://doi.org/10.1016/S0191-8141(96)00080-6.

Fallourd S, Poujol M, Boulvais P, Paquette J-L, de Saint Blanquat M, Remy P. 2014. Insitu LA-ICP-MS U-Pb titanite dating of Na-Ca metasomatism in orogenic belts; the North Pyrenean example. *International Journal of Earth Sciences* 103(3): 667–682. https://doi.org/10.1007/s00531-013-0978-1.

Fonteilles M, Machairas G. 1968. Eléments d'une description pétrographique et métallogénique du gisement de scheelite de Salau (Ariège) 2ème série. *Bulletin BRGM* 3: 62–85.

Fonteilles M, Nansot L, Soler P, Zahm A. 1988. Ore controls for the Salau Scheelite Deposit (Ariège, France): Evolution of ideas and present state of knowledge. Society of Geology Applied to Mineral Deposits Special Publication 6. Berlin-New York: Springer-Verlag, pp. 95–116.

Fonteilles M, Soler P, Demange M, Derré C, Krier-Schellen AD, Verkaeren J, *et al.* 1989. The scheelite skarn deposit of Salau (Ariège, French Pyrenees). *Economic Geology* 84: 1172–1209.

Fourel F, Lécuyer C, Martineau F, Seris M. 2014. Simultaneous N, C, S isotopic analyses using new purge and trap EA-IRMS technology. *Rapid Communications in Mass Spectrometry* 28: 2587–2594.

Gerbal A, Ledru P. 1985. Les indices de minéralisation à l'Est de la granodiorite de Salau : inventaire et cadre tectonométamorphique. Note technique BRGM 85-GEO-ET-57.

Gleizes G. 1992. Structure des granites hercyniens des Pyrénées de Mont-Louis-Andorre à la Maladeta. Thèse de 3e cycle de l'Université Sabatier de Toulouse, France.

Gleizes G, Leblanc D, Bouchez JL. 1997. Variscan granites of the Pyrenees revisited: their role as syntectonic markers of the orogen. *Terra Nova* 9(1): 38–41. https://doi.org/10.1046/j.13653121.1997.d01-9.x.

Gleizes G, Leblanc D, Santana V, Olivier P, Bouchez JL. 1998a. Sigmoidal structures featuring dextral shear during emplacement of the Hercynian granite complex of Cauterets-Panticosa (Pyrenees). *Journal of Structural Geology* 20(9-10): 1229–1245. https://doi.org/10.1016/S0191-8141(98)00060-1.

Gleizes G, Leblanc D, Bouchez JL. 1998b. The main phase of the Hercynian orogeny in the Pyrenees is a dextral transpression. *Geological Society of London Special Publication* 135(1): 267–273. https://doi.org/10.1144/GSL.SP1998.135.01.17.

Gleizes G, Leblanc D, Olivier P, Bouchez J. 2001. Strain partitioning in a pluton during emplacement in transpressional regime: the example of the Néouvielle granite (Pyrenees). *International Journal of Earth Sciences* 90(2): 325–340. https://doi.org/10.1007/s005310000144.

Gleizes G, Crevon G, Asrat A, Barbey P. 2006. Structure, age and mode of emplacement of the Hercynian Bordères-Louron pluton (Central Pyrenees, France). *International Journal of Earth Sciences* 95(6): 1039–1052. https://doi.org/insu.bib.cnrs.fr/10.1007/s00531-006-0088-4.

Goldschmidt VM. 1911. Die Kontaktmetamorphose in Kristianiagebiete. Skr. Norske Vidensk. −Akad. i Oslo, Mat.-na-turv. Kl., 11., 405 p.

Guiraudie C, Passaqui B, Prouhe, JP. 1964. Le gisement de tungstène (scheelite) de Salau (Ariège). Rapport BRGM DRMM-64-A2. Orléans, 95 p.

Guy B. 1979. Pétrologie et géochimie isotopique (S, C, O) des skarns de Costabonne. Thèse Doct. Ing. École des Mines de Paris.

Hammarstrom JM, Zen EA. 1986. Aluminum in hornblende; an empirical igneous geobarometer. *Am. Mineral.* 71(11-12): 1297–1313.

Harlaux M, Romer RL, Mercadier J, Morlot C, Marignac C, Cuney M. 2018. 40 Ma of hydrothermal W mineralization during the Variscan orogenic evolution of the French Massif Central revealed by U/Pb dating of wolframite. *Mineralium Deposita* 53(1): 21–51.

Harris M. 1980. Gold mineralization at the Salave gold prospect, north-west Spain: Institution of Mining and Metallurgy (London). *Transactions, Applied Earth Sciences*, sec. B, 89: B1–B4.

Harrison TM, Duncan I, McDougall I. 1985. Diffusion of ^{40}Ar in biotite: Temperature, pressure and compositional effects. *Geochimica et Cosmochimica Acta* 49: 2461–2468. https://doi.org/10.1016/0016-7037(85)90246-7.

Harrison TM, Celerier J, Aikman AB, Hermann J, Heizler MT. 2009. Diffusion of ^{40}Ar in muscovite. *Geochimica et Cosmochimica Acta* 73(4): 1039–1051. https://doi.org/10.1016/j.gca.2008.09.038.

Hart CJR., 2007. Reduced intrusion-related gold systems. In: Goodfellow, W.D. (Ed.) Mineral deposits of Canada: A Synthesis of Major Deposit Types, District Metallogeny, the Evolution of Geological Provinces, and Exploration Methods. *Geological Association of Canada*, Mineral Deposits Division, Special Publication 5: 95–112.

Hodgson CJ. 2000. Exploration Potential at Cantung Mine, District of Mackenzie, NWT. Andean Engineering.

Höll R, Ivanova G, Grinenko V. 1987. Sulfur isotope studies of the felbertal scheelite deposit, eastern Alps. *Mineralium Deposita* 22 (4): 301–308. https://doi.org/10.1007/BF00204523.

Hollister LS, Grissom GC, Peters EK, Stowell HH, Sisson VB. 1987. Confirmation of the empirical correlation of Al in hornblende with pressure of solidification of calc-alkaline plutons. *Am. Mineral.* 72 (3-4): 231–239.

Ishihara S, Sasaki A. 1989. Sulfur isotopic ratios of the magnetite-series and ilmenite-series granitoids of the Sierra Nevada batholith – A reconnaissance study. *Geology* 17: 788–791.

Jébrak M, Marcoux E. 2008. Géologie des ressources minérales. Ressources minérales et Faune, Québec. Bibliothèque et Archives nationales du Québec, 667 p.

Johnson MC, Rutherford MJ. 1989. Experimental calibration of the aluminum-in-hornblende geobarometer with application to Long Valley caldera (California) volcanic rocks. *Geology* 17(9): 837–841.

Jolivet M, Labaume P, Monié P, Brunel M, Arnaud N, Campani M. 2007. Thermochronology constraints for the propagation sequence of the south Pyrenean basement thrust system (France-Spain). *Tectonics* 26: TC5007. https://doi.org/10.1029/2006TC002080.

Kaelin JL. 1982. Analyse structurale du gisement de scheelite de Salau (Ariège, France). Thèse doct. Ing. ENSMP, Paris, 176 p.

Kesler SE, Riciputi LC, Ye Z. 2005. Evidence for a magmatic origin for Carlin-type gold deposits: isotopic composition of sulfur in the Betze-Post-Screamer Deposit, Nevada, USA. *Mineralium Deposita* 40: 127–136. https://doi.org/10.1007/s00126-005-0477-9.

Krier-Schellen AD. 1988. Etude microthermométrique des inclusions fluides des différentes paragenèses du gisement de scheelite (tungstène) de Salau (Pyrénées Ariégeoises, France). Thèse de l'Université Catholique de Louvain, La Neuve, 131 p.

Lancelot JR, Sarazin G, Allègre CJ. 1971. Composition isotopique du plomb et du soufre des galènes liées aux formations sédimentaires. Interprétations géologiques et géophysiques. *Contributions to Mineralogy and Petrology* 32: 315–333.

Lang JR, Baker T. 2001. Intrusion-related gold systems. The present level of understanding. *Mineralium Deposita* 36: 477–489.

Laumonier B, Marignac C, Kister P. 2010, Polymétamorphisme et évolution crustale dans les Pyrénées orientales pendant l'orogenèse varisque au Carbonifère supérieur. *Bulletin de la Société Géologique de France* 181(5): 411–428.

Lecouffe J. 1987. Les épisodes de fracturation dans le gisement de scheelite de Salau (Ariège), Caractères géométriques et pétrologiques, relation avec la minéralisation et implications minières. Thèse doct. Ing. ENSMP, Paris, 222 p.

Ledru P. 1986. Perspective d'extension du gisement de scheelite de Salau (Pyrénées Ariègeoises) : Données structurales. Rapport BRGM 86-SGN-063-GEO. Orléans, 22 p.

Ledru P, Autran A. 1987. Relationships between fluid circulation, ore deposition and shear zones: new evidence from the Salau scheelite deposit. *Economic Geology* 82: 224–229.

Lefebvre MG, Romer RL, Glodny J, Kroner U, Roscher M. 2018. The Hämmerlein skarn-hosted polymetallic deposit and the Eibenstock granite associated greisen, western Erzgebirge, Germany: two phases of mineralization – two Sn sources. *Mineralium Deposita* 126: 1–22. https://doi.org/10.1007/s00126-018-0830-4.

Lentz CPE, McFarlane CRM, Falck H. 2015. Petrogenetic controls on gold mineralization within the Amber Zone at Cantung W mine,

Northwest Territories, Canada. *Atlantic Geology* 51: 120–121. https://doi.org/10.4138/atlgeol.2015.005.

Link G, Vanderhaeghe O, Béziat D, de Saint Blanquat M, Munoz M, Estrade G, *et al.* 2019. Thermal peak detected in gold-bearing shear zones by a thermo-structural study: a new tool toretrieve fluid flow? In: *15th SGA Biennal Meeting on Life with Ore Deposits on Earth, Society for Geology Applied to Mineral Deposits, Aug. 2019*, Glasgow, United Kingdom, pp. 260–263.

Maloof TL, Baker T, Thompson JFN. 2001. The Dublin Gulch intrusion-related gold deposit, Tombstone Plutonic Suite, Yukon Territory, Canada. *Mineralium Deposita* 36: 583–593.

Mao M, Rukhlov AS, Rowins SM, Spence J, Coogan LA. 2016. Apatite trace element compositions: a robust new tool for mineral exploration. *Economic Geology* 111: 1187–1222.

Marcoux E, Nerci K, Branquet Y, Ramboz C, Ruffet G, Peucat JJ, *et al.* 2015. Late-Hercynian intrusion-related gold deposits: an integrated model on the Tighza polymetallic district, central Morocco. *Journal of African Earth Sciences* 107: 65–88. https://doi.org/10.1016/j.jafrearsci.2015.01.011.

Massone HJ, Schreyer R. 1987. Phengite geobarometry based on the limiting assemblage with K-feldspar, phlogopite, and quartz. *Contributions to Mineralogy and Petrology* 96: 212–224.

Maurel O, Monié P, Pik R, Arnaud N, Brunel M, Jolivet M. 2008. The Meso-Cenozoic thermo-tectonic evolution of the Eastern Pyrenees: an $^{40}Ar/^{39}Ar$ fission track and (U-Th)/He thermochronological study of the Canigou and Mont-Louis massifs. *International Journal of Earth Sciences* 97: 565–584. https://doi.org/10.1007/s00531-007-0179-x.

McCaig A, Miller JA. 1986. $^{40}Ar/^{39}Ar$ age of mylonites along the Mérens fault, Central Pyrenees. *Tectonophysics* 129: 149–172. https://doi.org/10.1016/0040-1951(86)90250-7.

Meinert LD, Dipple GM, Nicolesku S. 2005. World skarn deposits. *Economic Geology* 100: 299–336.

Metcalf JR, Fitzgerald PG, Baldwin SL, Muñoz JA. 2009. Thermochronology of a convergent orogen: Constraints on the timing of thrust faulting and subsequent exhumation of the Maladeta Pluton in the Central Pyrenean Axial Zone. *Earth and Planetary Sciences Letters* 287(3-4): 488–503. https://doi.org/10.1016/j.epsl.2009.08.036.

Mezger J.E. 2009. Transpressional tectonic setting during the main Variscan deformation: evidence from four structural levels in the Bossòst and Aston-Hospitalet mantled gneiss domes, central Axial Zone, Pyrenees. *Bulletin de la Société Géologique de France* 180 (3): 199–207. https://doi.org/10.2113/gssgfbull.180.3.199.

Mezger JE, Schnapperelle S, Rölke C. 2012. Evolution of the Central Pyrenean Mérens fault controlled by near collision of two gneiss domes. *Hallesches Jahrb. Für Geowiss* 34(0): 11–30.

Michard AG, Bouquet C. 1986. Inventaire du territoire métropolitain, recherches de tungstène dans la haute vallée du Salat (Ariège), historique et bilan des travaux à fin 1985. Rapport BRGM 86-DAM-008-OP4. Orléans, 18 p.

Monié P, Soliva J, Brunel M, Maluski H. 1994. Les cisaillements mylonitiques du granite de Millas (Pyrénées, France). Age Crétacé 40Ar/39Ar et interprétation tectonique. *Bulletin de la Société Géologique de France* 165: 559–571.

Monier G, Robert JL. 1986. Muscovite solid solutions in the system K_2O–Mgo–FeO–Al_2O_3–SiO_2–H_2O: an experimental study at 2 kbar PH2O and comparison with natural Li-free white micas. *Mineralogical Magazine* 50: 257–266.

Mustard R. 2001. Granite-hosted gold mineralization at Timbarra, northern New South Wales, Australia. *Mineralium Deposita* 36(6): 542–562.

Mutch EJF, Blundy JD, Tattitch BC, Cooper FJ, Brooker RA. 2016. An experimental study of amphibole stability in low-pressure granitic magmas and a revised Al-in-hornblende geobarometer. *Contrib. Mineral. Petrol.* 171(85). https://doi.org/10.1007/s00410-016-1298-9.

Olivier P, Gleizes G, Paquette JL, Muñóz Sáez C. 2008. Structure and U-Pb dating of the Saint-Arnac pluton and the Ansignan charnockite (Agly Massif): a cross-section from the upper to the middle crust of the Variscan Eastern Pyrenees. *Journal of the Geological Society, London* 165:141–152.

Olivier P, Druguet E, Castano LM, Gleizes G. 2016. Granitoid emplacement by multiple sheeting during Variscan dextral transpression; the Saint-Laurent-La Jonquera Pluton (eastern Pyrenees). *Journal of Structural Geology* 82: 80–92. https://doi.org/10.1016/j.jsg.2015.10.006.

Palau i Ramirez J, Arcos D, Delgado J, Soler A. 1995. Gold-bearing metasomatic bodies related to the Hercynian plutonism in the Marimanya area (Central Pyrenees, Spain). In: *Mineral Deposits: From Their Origin to Their Environmental Impacts*, pp. 493–496.

Palau i Ramirez J, Soler A, Solé J, Espinola MR, Delgado J. 1997. Dating of gold-bearing skarns and intragranitic mineralizations in the Central Pyrenees. A new approach to thematic mapping. In: *Second Congress on Regional Geological Cartography and Information Systems*, pp. 53–58.

Palmer EM, McFarlane CRM, Lentz DR, Falck H. 2013. Gold in the Cantung W skarn deposit, Northwest Territories: distribution, mineralogy, and paragenesis. *Atlantic Geology* 49: 174–175.

Passaqui B, Costargent R. 1965. Gisement de scheelite de Salau (Ariège), résultats de la campagne 1964. Rapport BRGM DRMM-65-A6. Orléans, 13 p.

Paquette J-L, Gleizes G, Leblanc D, Bouchez JL. 1997. Le granite de Bassiès (Pyrénées) : un pluton syntectonique d'âge Westphalien. Géochronologie U-Pb sur zircons. *Comptes Rendus de l'Académie des Sciences* 324(IIa): 387–392.

Poitrenaud T. 2018. Le gisement périgranitique à tungstène et or de Salau (Pyrénées, France), histoire polyphasée d'un système minéralisé tardi-varisque. Thèse de l'Université d'Orléans, 490 p.

Poitrenaud T, Poujol M, Augier R, Marcoux E. 2019. The polyphase evolution of a late Variscan W/Au deposit (Salau, French Pyrenees): insights from REE and U/Pb LA-ICP-MS analyses. *Mineralium Deposita*. https://doi.org/10.1007/s00126-019-00923-2.

Pouit G. 1984. Les gisements à sulfures massifs exhalatifs-sédimentaires : une mise au point sur leur classification et la méthodologie de leur recherche. *Chronique de la Recherche Minière* 476: 31–34.

Poujol M, Boulvais P, Kosler J. 2010. Regional-scale Cretaceous albitization in the Pyrenees; evidence from in situ U-Th-Pb dating of monazite, titanite and zircon. *Journal of the Geological Society, London* 167(4): 751–767. https://doi.org/10.1144/0016-76492009-144.

Prouhet JP, Guiraudie C, Passaqui B, Costargent R. 1966. Gisement de scheelite de Salau (Ariège), résultats en fin de campagne 1965. Rapport BRGM DRMM-66-A5. Orléans, 44 p.

Pura A, Canet C, Melgarejo JC, Fallick AE. 2002. Sulphur isotope composition of Silurian shale-hosted PGE-Ag-Au-Zn-Cu mineralisations of the Prades Mountains (Catalonia, Spain). *Mineralium Deposita* 37(2): 198–212. https://doi.org/10.1007/s00126-001-0217-8.

Raimbault L. 1981. Pétrographie et géochimie des roches du massif granodioritique de Salau (Pyrénées). Rapport de l'École des Mines de Saint-Etienne, 85 p.

Raju PVS, Hart CJR, Sangurmath P. 2015. Scheelite geochemical signatures by LA-ICP-MS and potential for rare earth elements from Hutti Gold Mines and fingerprinting ore deposits. *Journal of African Earth Sciences* 114: 220–227.

Rasmussen KL. 2004. The aplitic dykes of the Cantung Mine, NWT: Petrology, geochemistry, and implications for the mineralization process. Unpublished B.Sc. Thesis, Department of Geology and Geophysics, The University of Calgary, Calgary, Alberta, Canada.

Rasmussen KL, Lentz DR, Falck H, Pattison DRM. 2011. Felsic magmatic phases and the role of late-stage aplitic dikes in the formation of the world class Cantung tungsten skarn deposit, Northwest Territories, Canada. *Ore Geology Reviews* 41: 75–111.

Roberts MP, Pin C, Clemens JD, Paquette J-L. 2000. Petrogenesis of mafic to felsic plutonic rock associations: the calc-alkaline Quérigut Complex, French Pyrenees. *Journal of Petrology* 41 (6): 809–844. https://doi.org/10.1093/petrology/41.6.809.

Romer RL, Soler A. 1995. U-Pb age and lead isotopic characterization of Au-bearing skarn related to Andorra granite (Pyrenees, Spain). *Mineralium Deposita* 30: 374–383.

Rye RO, Ohmoto H. 1974. Sulfur and carbon isotopes and ore genesis: A review. *Economic Geology* 69: 826–842.

Schmidt MW. 1992. Amphibole composition in tonalite as a function of pressure: an experimental calibration of the Al-in-hornblende barometer. *Contrib. Mineral. Petrol.* 110(2-3): 304–310.

Seal RR. 2006. Sulfur isotope geochemistry of sulfide minerals. *Reviews in Mineralogy and Geochemistry* 61: 633–677.

Sharman ER, Bruce T, Minarik W, Dubé B, Boswell AW. 2014. Sulfur isotope and trace element data from ore sulfides in the Noranda district (Abitibi, Canada): implications for volcanogenic massive sulfide deposit genesis. *Mineralium Deposita* 50: 591–606. https://doi.org/10.1007/s00126-014-0559-7.

Sitter de LU, Zwart HJ. 1960. Tectonic development in supra and infra-structures of a mountain chain. In: *Proc. 21st International Congress of Copenhagen* 18: 248–256.

Soler P. 1977. Pétrographie, thermochimie et métallogénie du gisement de scheelite de Salau (Pyrénées ariègeoises, France). Thèse doct. Ing. ENSMP, Paris, 270 p.

Soler A. 1990. Geologia i metallogenia de la terminacio sud del granit d'Andorra (Pirineu Central). Tesis doctoral, Universitat de Barcelona, 886 p.

Soler A, Ayora C, Cardellach E, Delgado J. 1990. Gold-bearing hedenbergite skarns from the SW contact of the Andorra Granite (central Pyrenees, Spain). *Mineralium Deposita* 25: 59–68.

Soloviev SG, Kryazhev SG, Dvurechenskaya SS. 2017a. Geology, mineralization, and fluid inclusion characteristics of the Lermontovskoe reduced-type tungsten (± Cu, Au, Bi) skarn deposit, Sikhote-Alin, Russia. *Ore Geology Reviews* 89: 15–39. https://doi.org/10.1016/j.oregeorev.2017.06.002.

Soloviev SG, Kryazhev SG, Dvurechenskaya SS. 2017b. Geology, mineralization, stable isotope, and fluid inclusion characteristics of the Vostok-2 reduced W-Cu skarn and Au-W-Bi-As stockwork deposit, Sikhote-Alin, Russia. *Ore Geology Reviews* 86: 338–365. https://doi.org/10.1016/j.oregeorev.2017.02.029.

Soloviev SG, Kryazhev SG. 2017c. Geology, mineralization, and fluid inclusion characteristics of the Skrytoe reduced-type W skarn and stockwork deposit, Sikhote-Alin, Russia. *Mineralium Deposita* 52: 903–928. https://doi.org/10.1007/s00126-016-0705-1.

Tanner D, Henley RW, Mavrogenes JA, Holden P. 2016. Sulfur isotope and trace element systematics of zoned pyrite crystals from the El Indio Au-Cu-Ag deposit, Chile. *Contributions to Mineralogy and Petrology* 171(4): 1–17.

Thomas W, Ernst WG. 1990. The aluminum content of hornblende in calc-alkaline granitic rocks; a mineralogic barometer calibrated experimentally to 12 kbars. In: Spencer RJ, Chou IM, (eds). *Fluid–Mineral Interactions: A Tribute to H.P. Eugster*. Geochem. Soc. Spec. Publ. 2: 59–63.

Thompson JFG, Sillitoe RH, Baker T, Lang JR, Mortensen JK. 1999. Intrusion related gold deposits associated with tungsten-tin provinces. *Mineralium Deposita* 34: 323–344.

Thompson JFH, Newberry RJ. 2000. Gold deposits related to reduced granitic intrusions. *Reviews in Economic Geology* 13: 377–400.

Toulhoat P. 1982. Pétrographie et géochimie des isotopes stables (D/H, $^{18}O/^{16}O$, $^{13}C/^{12}C$, $^{34}S/^{32}S$) des skarns du Quérigut. Comparaison avec les skarns à scheelite des Pyrénées. Thèse d'Université Paris VI.

Uchida E, Endo S, Makino M. 2007. Relationship between solidification depth of granitic rocks and formation of hydrothermal ore deposits. *Resource Geology* 57(1): 47–56.

Van den Eeckhout B, de Bresser H. 2014. On the dextral offset of a Variscan shear zone across the Mérens fault in the central Pyrenees (Andorra, France). *Bulletin de la Société Géologique de France* 185(2): 131–143. https://doi.org/10.2113/gssgfbull.185.2.131.

Velde B. 1965. Phengitic micas: synthesis, stability and natural occurrence. *American Journal of Science* 263: 886–913.

Villa IM. 1998. Isotopic closure. *Terra Nova* 10: 42–47.

Vissers RLM, van Hinsbergen DJJ, Wilkinson CM, Ganerød M. 2017. Middle Jurassic shear zones at Cap de Creus (eastern Pyrenees, Spain): a record of pre-drift extension of the Piemonte-Ligurian Ocean? *Journal of the Geological Society, London* 174: 289–300. https://doi.org/10.1144/jgs2016-014.

Wayne DM, McCaig AM. 1998. Dating fluid flow in shear zones: Rb–Sr and U–Pb studies of syntectonic veins in the Néouvielle Massif, Pyrenees. In: Parnell J, ed. *Dating and Duration of Fluid Flow and Fluid–Rock Interaction*. Geological Society of London, Special Publications 144: 129–135. https://doi.org/10.1144/GSL.SP.1998.144.01.09.

Yang XM, Lentz DR. 2010. Sulfur isotopic systematics of granitoids from southwestern New Brunswick, Canada; implications for magmatic-hydrothermal processes, redox conditions, and gold mineralization. *Mineralium Deposita* 45: 795–816. https://doi.org/10.1007/s00126-010-0307-6.

Zahm A. 1987. Pétrographie, minéralogie et géochimie des cornéennes calciques et des skarns dans le gisement de scheelite de Salau (Ariège, France). Thèse d'Université Paris VI, 384 p.

Zhang W, Williams-Jones AE, Leng CB, Zhang XC, Chen WT, Qin CJ, *et al.* 2019. The origin of CH_4-rich fluids in reduced porphyry-skarn Cu-Mo-Au systems. *Ore Geology Reviews* 114: 103–135. https://doi.org/10.1016/j.oregeorev.2019.103135.

Zwart HJ. 1979. The geology of the Central Pyrenees. *Leidse Geol. Meded.* 50: 1–74.

Cite this article as: Poitrenaud T, Marcoux É, Augier R, Poujol M. 2021. The perigranitic W-Au Salau deposit (Pyrenees, France): polyphase genesis of a late Variscan intrusion related deposit, *BSGF - Earth Sciences Bulletin* 192: 22.